BUCKLING BEHAVIOR OF LONG ANISOTROPIC PLATES SUBJECTED TO FULLY RESTRAINED THERMAL EXPANSION

Michael P. Nemeth*
Mechanics and Durability Branch, NASA Langley Research Center
Hampton, Virginia 23681-2199

Abstract

An approach for synthesizing buckling results and behavior for thin balanced and unbalanced symmetric laminates that are subjected to uniform heating or cooling and fully restrained against thermal expansion or contraction is presented. This approach uses a nondimensional analysis for infinitely long, flexurally anisotropic plates that are subjected to combined mechanical loads and is based on useful nondimensional parameters. In addition, stiffness-weighted laminate thermal-expansion parameters are derived that are used to determine critical temperatures in terms of physically intuitive mechanical buckling coefficients, and the effects of membrane orthotropy and membrane anisotropy are included. Many results are presented for some common laminates that are intended to facilitate a structural designer's transition to the use of the generic buckling design curves that are presented in the paper. Several generic buckling design curves are presented that provide physical insight into the buckling response in addition to providing useful design data. Examples are presented that demonstrate the use of the generic design curves. The analysis approach and generic results indicate the effects and characteristics of laminate thermal expansion, membrane orthotropy and anisotropy, and flexural orthotropy and anisotropy in a very general and unifying manner.

Introduction

Buckling behavior of laminated-composite plates that are subjected to combined mechanical and thermal loads is an important consideration in the preliminary design of contemporary, high-performance aerospace vehicles. The sizing of many structural subcomponents of these vehicles is often determined by buckling constraints. One subcomponent that is of practical importance in structural design is the long rectangular plate. These plates commonly appear as elements of stiffened panels that are used for wing structures, and as semimonocoque shell segments that are used for fuselage structures. Buckling results for infinitely long plates are important because they often provide a practical estimate of the behavior of finite-length rectangular plates, and they provide information that is useful in explaining the behavior of these finite-length plates. Moreover, knowledge of the behavior of infinitely long plates can provide insight into the buckling behavior of more complex structures such as stiffened panels.

An important type of long plate that appears as a component of contemporary composite structures is the symmetrically laminated plate. In the present paper, the term, "symmetrically laminated," refers to plates in which every lamina above the plate midplane has a corresponding lamina located at the same distance below the plate midplane, with the same thickness, material properties, and fiber orientation. Symmetrically laminated plates are essentially flat after the manufacturing process and exhibit flat prebuckling deformation states, which is desirable for many applications. More importantly, the amenability of these plates to structural tailoring provides symmetrically laminated plates with a significant potential for reducing the weight of aerospace vehicles or for meeting special performance requirements. Thus, understanding the buckling behavior of symmetrically laminated plates in a very broad manner is an important part of the search for ways to exploit plate orthotropy and anisotropy to reduce structural weight or to fulfil a special design requirement.

For many practical cases, symmetrically laminated plates exhibit specially orthotropic behavior. However, in some cases, such as thin-walled $[\pm 45]_s$ laminates that are candidates for spacecraft applications, these plates exhibit anisotropy in the form of material-induced coupling between pure bending and twisting deformations. This coupling is referred to herein as flexural anisotropy and it generally yields buckling modes that are skewed in appearance (see Fig. 1), even when inplane shear loads are absent. Symmetrically laminated plates that are unbalanced are also being investigated for special-purpose uses in aerospace structures. These laminated plates exhibit anisotropy in the form of material-induced coupling between pure inplane dilatation and inplane shear deformations, in addition to flexural anisotropy. This coupling is referred to herein as membrane anisotropy and it generally yields combined inplane stress states for simple loadings like uniform edge compression when inplane displacement constraints are imposed on one or more edges of a plate. For example, when the edges of

* Senior Research Engineer and Assistant Head. Associate Fellow, AIAA.

an unbalanced, symmetrically laminated plate, such as a $[+45_2/0/90]_s$ laminate, are totally restrained against thermal expansion and contraction, that is caused by uniform heating or cooling, inplane shear stresses are developed in addition to the usual compressive stresses that are often present in balanced laminates. These kinematically induced shear stresses may be relatively large in magnitude, compared to the direct compressive stresses, and as a result may greatly affect the buckling behavior of the plate and yield buckling modes that are skewed in appearance.

The effects of flexural orthotropy and flexural anisotropy on the buckling behavior of long rectangular plates that are subjected to single and combined mechanical loading conditions are becoming better understood. For example, recent in-depth parametric studies that show the effects of flexural orthotropy and flexural anisotropy on the buckling behavior of long plates that are subjected to compression, shear, pure inplane bending, and various combinations of these loads have been presented in Refs. 1-3. The results presented in these references indicate that the importance of flexural anisotropy on the buckling resistance of long plates varies with the magnitude and type of the combined loading condition. Similar results for plates loaded by uniform shear and a general linear distribution of axial load across the plate width have also been presented in Ref. 4. In a similar manner, the effects of membrane orthotropy and membrane anisotropy on the buckling behavior of long rectangular plates that are restrained against axial thermal expansion and contraction and subjected to uniform heating or cooling and mechanical loads have been presented in Ref. 5. This extensive work has provided a better understanding of the load interaction effects of balanced and unbalanced, symmetrically laminated plates that are subjected to mechanical loads and restrained against axial thermal expansion and contraction.

Although an extensive body of work exists that addresses the thermal-buckling behavior of plates (see Ref. 5 for a literature review), a broad understanding of the effects of orthotropy and anisotropy on their response has not yet been obtained. In particular, the effects of membrane orthotropy and membrane anisotropy on the buckling behavior of long rectangular plates that are fully restrained against thermal expansion and contraction and subjected to uniform heating or cooling are not well understood for the large variety of laminated plates that exist and the variety of support conditions that are possible. One objective of the present paper is to present a more intuitive buckling analysis for balanced and unbalanced, symmetrically laminated plates, that are fully restrained against thermal expansion and contraction and subjected to uniform heating or cooling. To achieve this goal, the buckling analysis is formulated in terms of buckling coefficients for the known, mechanically equivalent loads and stiffness-weighted laminate thermal-expansion parameters instead of a less intuitive thermal buckling coefficient. Thus, the present study is a continuation or extension of the work that is presented in Ref. 5. The analysis procedure is based on classical laminated-plate theory, which neglects transverse-shear flexibility, and is applied to long plates herein. However, the analysis procedure is applicable to finite-length plates and to more sophisticated plate buckling theories that include effects like transverse shear flexibility.

Two other objectives of the present paper are to present a wide range of buckling results in terms of useful nondimensional design parameters and to provide a means for comparing the buckling-response characteristics of seemingly dissimilar laminated plates. Other objectives are to identify the effects of orthotropy and anisotropy on the buckling behavior of long symmetrically laminated plates that are subjected to the same loading conditions, and to present some previously unknown results. In particular, results are presented for plates with the two long edges clamped or simply supported and all edges fully restrained against inplane movement. Several generic buckling-design curves that are applicable to a wide range of laminate constructions are presented that use the nondimensional parameters described in Refs. 1-6, along with some other parameters that are derived subsequently. Finally, examples are presented that demonstrate the use of the generic buckling design curves and the analysis procedure.

Analysis Description

In preparing generic design charts for buckling of a single flat thin plate, a special-purpose analysis is often preferred over a general-purpose analysis code, such as a finite-element code, because of the cost and effort that is usually involved in generating a large number of results with a general-purpose code. The results to be presented in the proposed paper were obtained by using such a special-purpose buckling analysis that is based on classical laminated-plate theory. The analysis details are lengthy; hence, only a brief description of the buckling analysis is presented herein. First, the buckling analysis for long plates that are subjected to a general set of mechanical loads is described. Then, the mechanical loads that are induced by fully restrained thermal expansion and contraction and that are used in the buckling analysis are derived, and an expression for the critical temperature change is presented that is in terms of the corresponding crtitical loading parameter and mechanical-buckling coefficients.

Buckling Analysis

Symmetrically laminated plates can have many dif-

ferent constructions because of the wide variety of material systems, fiber orientations, and stacking sequences that can be selected to construct a laminate. A way of coping with the large number of choices for laminate constructions is to use convenient nondimensional parameters in order to understand overall behavioral trends and sensitivities of the structural behavior to perturbations in laminate construction. The buckling analysis used in the present paper is based on classical laminated-plate theory and the classical Rayleigh-Ritz method, and is derived explicitly in terms of the nondimensional parameters defined in Refs. 1-6. This approach was motivated by the need for generic (independent of a specific laminate construction) parametric results for composite-plate buckling behavior that are expressed in terms of the minimum number of independent parameters needed to fully characterize the behavior, and that indicate the overall trends and sensitivity of the results to changes in the parameters. The nondimensional parameters that were used to formulate the buckling analysis are given by

$$\alpha_{\sim} = \frac{b}{\lambda}\left(\frac{D_{11}}{D_{22}}\right)^{1/4} \tag{1}$$

$$\beta = \frac{D_{12} + 2D_{66}}{(D_{11} D_{22})^{1/2}} \tag{2}$$

$$\gamma = \frac{D_{16}}{(D_{11}^3 D_{22})^{1/4}} \tag{3}$$

$$\delta = \frac{D_{26}}{(D_{11} D_{22}^3)^{1/4}} \tag{4}$$

where b is the plate width and λ is the half-wave length of the buckle pattern of an infinitely long plate (see Fig. 1). The subscripted D-terms are the bending stiffnesses of classical laminated-plate theory. The parameters $\alpha_{\sim}$ and β characterize the flexural orthotropy, and the parameters γ and δ characterize the flexural anisotropy.

The mechanical loading conditions that are included in the buckling analysis are uniform transverse tension or compression, uniform shear, and a general linear distribution of axial load across the plate width, as depicted in Fig. 1. Typically, an axial stress resultant distribution is partitioned into a uniform part and a pure bending part. However, this representation is not unique. The longitudinal stress resultant N_x is partitioned in the analysis into a uniform tension or compression part and a linearly varying part that corresponds to eccentric inplane bending loads. This partitioning is given by

$$N_x = N_{xc} - N_b\left[\varepsilon_0 + (\varepsilon_1 - \varepsilon_0)\eta\right] \tag{5}$$

where N_{xc} denotes the intensity of the constant-valued tension or compression part of the load, and the term containing N_b defines the intensity of the eccentric inplane bending load distribution. The symbols ε_0 and ε_1 define the distribution of the inplane bending load, and the symbol η is the nondimensional coordinate given by $\eta = y/b$. This particular way of partitioning the longitudinal stress resultant was used for convenience by eliminating the need to calculate the uniform and pure bending parts of an axial stress resultant distribution prior to performing a buckling analysis.

The analysis is based on a general formulation that includes combined destabilizing loads that are proportional to a positive-valued loading parameter $\bar{p}$ that is increased until buckling occurs, and independent subcritical combined loads that remain fixed at a specified load level below the value of the buckling load. Herein, the term "subcritical load" is defined as any load that does not cause buckling to occur. In practice, the subcritical loads are applied to a plate prior to, and independent of, the destabilizing loads with an intensity below that which will cause the plate to buckle. Then, with the subcritical loads fixed, the active, destabilizing loads are applied by increasing the magnitude of the loading parameter until buckling occurs. This approach permits certain types of combined-load interaction to be investigated in a direct and convenient manner. For example, in analyzing the stability of an aircraft fuselage, the nondestabilizing transverse tension load in a fuselage panel that is caused by cabin pressurization can be considered to remain constant and, as a result, it can be represented as a passive, subcritical load. The combined shear, compression, and inplane bending loads that are caused by flight maneuvers can vary and cause buckling and, as a result, they can be represented as active, destabilizing loads.

The distinction between the active, destabilizing and passive subcritical loading systems is implemented in the buckling analysis by partitioning the prebuckling stress resultants as follows

$$N_{xc} = -N_{x1}^c + N_{x2}^c \tag{6}$$

$$N_y = -N_{y1} + N_{y2} \tag{7}$$

$$N_{xy} = N_{xy1} + N_{xy2} \tag{8}$$

$$N_b = N_{b1} + N_{b2} \tag{9}$$

where the stress resultants with the subscript 1 are the destabilizing loads, and those with the subscript 2 are the subcritical loads. The sign convention used herein for positive values of these stress resultants is shown in Fig. 1. In particular, positive values of the general linear

edge stress distribution parameters N_{b1}, N_{b2}, ε_0, and ε_1 correspond to compression loads. Negative values of N_{b1} and N_{b2}, or negative values of either ε_0 or ε_1, yield linearly varying stress distributions that include tension. Depictions of a variety of inplane bending load distributions are given in Ref. 4. The two normal stress resultants of the system of destabilizing loads, N^c_{x1} and N_{y1}, are defined to be positive-valued for compression loads. This convention results in positive eigenvalues being used to indicate instability due to uniform compression loads.

The buckling analysis includes several nondimensional stress resultants associated with Eqs. (6) through (9). These dimensionless stress resultants are given by

$$n^c_{xj} = \frac{N^c_{xj}\, b^2}{\pi^2 (D_{11}\, D_{22})^{1/2}} \tag{10}$$

$$n_{yj} = \frac{N_{yj}\, b^2}{\pi^2\, D_{22}} \tag{11}$$

$$n_{xyj} = \frac{N_{xyj}\, b^2}{\pi^2 (D_{11}\, D^3_{22})^{1/4}} \tag{12}$$

$$n_{bj} = \frac{N_{bj}\, b^2}{\pi^2 (D_{11}\, D_{22})^{1/2}} \tag{13}$$

where the subscript j takes on the values of 1 and 2. In addition, the destabilizing loads are expressed in terms of the loading parameter $\tilde{p}$ in the analysis by

$$n^c_{x1} = L_1\, \tilde{p} \tag{14}$$

$$n_{y1} = L_2\, \tilde{p} \tag{15}$$

$$n_{xy1} = L_3\, \tilde{p} \tag{16}$$

$$n_{b1} = L_4\, \tilde{p} \tag{17}$$

where L_1 through L_4 are load factors that determine the specific form (relative contributions of the load components) of a given system of destabilizing loads. Typically, the dominant load factor is assigned a value of 1 and all others are given as positive or negative fractions.

Nondimensional buckling coefficients that are used herein are given by the values of the dimensionless stress resultants of the system of destabilizing loads at the onset of buckling; i.e.,

$$K_x \equiv \left(n^c_{x1} \right)_{cr} = \frac{\left(N^c_{x1} \right)_{cr} b^2}{\pi^2 (D_{11}\, D_{22})^{1/2}} = L_1\, \tilde{p}_{cr} \tag{18}$$

$$K_y \equiv \left(n_{y1} \right)_{cr} = \frac{\left(N_{y1} \right)_{cr} b^2}{\pi^2 D_{22}} = L_2\, \tilde{p}_{cr} \tag{19}$$

$$K_s \equiv \left(n_{xy1} \right)_{cr} = \frac{\left(N_{xy1} \right)_{cr} b^2}{\pi^2 (D_{11}\, D^3_{22})^{1/4}} = L_3\, \tilde{p}_{cr} \tag{20}$$

$$K_b \equiv \left(n_{b1} \right)_{cr} = \frac{\left(N_{b1} \right)_{cr} b^2}{\pi^2 (D_{11}\, D_{22})^{1/2}} = L_4\, \tilde{p}_{cr} \tag{21}$$

where the quantities enclosed in the parentheses with the subscript "cr" are critical values that correspond to buckling and $\tilde{p}_{cr}$ is the magnitude of the loading parameter at buckling. Positive values of the coefficients K_x and K_y correspond to uniform compression loads, and the coefficient K_s corresponds to uniform positive shear. The direction of a positive shear stress resultant that acts on a plate is shown in Fig. 1. The coefficient K_b corresponds to the specific inplane bending load distribution defined by the selected values of the parameters ε_0 and ε_1 (see Fig. 1).

The mathematical expression used in the variational analysis to represent the general off-center and skewed buckle pattern is given by

$$w_N(\xi,\eta) = \sum_{m=1}^{N} \left(A_m \sin m\pi\xi + B_m \cos m\pi\xi \right) \Phi_m(\eta) \tag{22}$$

where $\xi = x/\lambda$ and $\eta = y/b$ are nondimensional coordinates, w_N is the out-of-plane displacement field, and A_m and B_m are the unknown displacement amplitudes. In accordance with the Rayleigh-Ritz method, the basis functions $\Phi_m(\eta)$ are required to satisfy the kinematic boundary conditions on the plate edges at η = 0 and 1. For the simply supported plates, the basis functions used in the analysis are given by

$$\Phi_m(\eta) = \sin m\pi\eta \tag{23}$$

for values of m = 1, 2, 3, ..., N. Similarly, for the clamped plates, the basis functions are given by

$$\Phi_m(\eta) = \cos(m-1)\pi\eta - \cos(m+1)\pi\eta \tag{24}$$

For both boundary conditions, the two long edges of a plate are free to move in-plane.

Algebraic equations that govern the buckling behavior of infinitely long plates are obtained by substituting the series expansion for the buckling mode given by Eq. (22) into a nondimensionalized form of the second variation of the total potential energy and then computing the integrals appearing in the nondimensional second variation in closed form. The resulting equations constitute a generalized eigenvalue problem that depends on

the aspect ratio of the buckle pattern λ/b (see Fig. 1) and the nondimensional parameters and nondimensional stress resultants defined herein. The smallest eigenvalue of the problem corresponds to buckling and is found by specifying a value of λ/b and solving the corresponding generalized eigenvalue problem for its smallest eigenvalue. This process is repeated for successive values of λ/b until the overall smallest eigenvalue is found.

Results that were obtained from the analysis described herein for uniform compression, uniform shear, pure inplane bending (given by $\varepsilon_0 = -1$ and $\varepsilon_1 = 1$), and various combinations of these mechanical loads have been compared with other results for isotropic, orthotropic, and anisotropic plates that were obtained by using other analysis methods. These comparisons are discussed in Refs. 1-3, and in every case the results described herein were found to be in good agreement with those obtained from other analyses. Likewise, results were obtained for isotropic and specially orthotropic plates that are subjected to a general linear distribution of axial load across the plate width and compared with results that were obtained by seven different authors (see Ref. 4). In every case, the agreement was good.

Prebuckling Stresses and Critical Temperature Change

Uniformly heated or cooled plates that are symmetrically laminated and restrained against thermal expansion and contraction may develop internal mechanical loads that can cause buckling. These induced mechanical loads enter the analysis through the membrane constitutive equations. The standard form of these membrane constitutive equations for thin plates, that is based on classical laminated-plate theory, is found in Refs. 7 and 8 and is expressed in terms of membrane stiffness coefficients and fictitious thermal stress resultants. In the present study, the membrane constitutive equations are used in an inverted form that uses the overall laminate coefficients of thermal expansion and the membrane compliance coefficients (see Ref. 8). This form of the membrane constitutive equations for symmetrically laminated plates is given by

$$\begin{Bmatrix} u_{,x} \\ v_{,y} \\ u_{,y} + v_{,x} \end{Bmatrix} = \begin{bmatrix} a_{11} & a_{12} & a_{16} \\ a_{12} & a_{22} & a_{26} \\ a_{16} & a_{26} & a_{66} \end{bmatrix} \begin{Bmatrix} N_x \\ N_y \\ N_{xy} \end{Bmatrix} + \begin{Bmatrix} \alpha_x \\ \alpha_y \\ \alpha_{xy} \end{Bmatrix} \Theta_0 \qquad (25)$$

where u(x,y) and v(x,y) are the prebuckling, inplane displacements in the x- and y-coordinate directions (see Fig. 2), respectively; α_x, α_y, and α_{xy} are the overall laminate coefficients of thermal expansion; the subscripted a-terms are the plate membrane compliance coefficients; Θ_0 is the magnitude of the uniform temperature change from a predetermined stress- and strain-free reference state; and commas followed by a subscript denote partial differentiation with respect to the coordinate associated with the subscript. For restrained thermal expansion and contraction problems, the plates are assumed to be supported and loaded such that the prebuckling stress field is uniform, that is, homogeneous. With this assumption, a compatible displacement field is obtained directly by integrating Eqs. (25). This integration yields

$$u(x,y) = \left(a_{11} N_x + a_{12} N_y + a_{16} N_{xy} + \alpha_x \Theta_0\right)x + g_1 y + g_2 \qquad (26)$$

$$v(x,y) = \left(a_{12} N_x + a_{22} N_y + a_{26} N_{xy} + \alpha_y \Theta_0\right)y + g_3 x + g_4 \qquad (27)$$

and

$$g_1 + g_3 = a_{16} N_x + a_{26} N_y + a_{66} N_{xy} + \alpha_{xy} \Theta_0 \qquad (28)$$

Equations (26)-(28) can be used to determine the thermally induced mechanical loadings for several problems of practical interest. The problems consist of plates restrained against axial thermal expansion or contraction (see Ref. 5), plates restrained against transverse thermal expansion or contraction (y-coordinate direction), and plates restrained against axial and transverse thermal expansion and contraction. In the present paper, however, only plates that are fully restrained against axial and transverse thermal expansion and contraction are considered. For this case, all the subcritical loads are zero-valued and $N_x(x,y) = -N^c_{x1}$, $N_y(x,y) = -N_{y1}$, and $N_{xy}(x,y) = N_{xy1}$ (see Fig. 2). All the stress resultants are induced by the fully restrained thermal expansion and contraction and, when considered together, are destabilizing. The displacements given by Eqs. (26) and (27) become

$$u(x,y) = \left(-a_{11} N^c_{x1} - a_{12} N_{y1} + a_{16} N_{xy1} + \alpha_x \Theta_0\right)x + g_1 y + g_2 \qquad (29)$$

$$v(x,y) = \left(-a_{12} N^c_{x1} - a_{22} N_{y1} + a_{26} N_{xy1} + \alpha_y \Theta_0\right)y + g_3 x + g_4 \qquad (30)$$

and Eq. (28) becomes

$$g_1 + g_3 = -a_{16} N^c_{x1} - a_{26} N_{y1} + a_{66} N_{xy1} + \alpha_{xy} \Theta_0 \qquad (31)$$

Enforcing the restraint condition (displacement boundary condition) $u(0,y) = 0$ gives $g_1 = g_2 = 0$. Similarly, enforcing the restraint condition $v(x,0) = 0$ gives $g_3 = g_4 = 0$. Enforcing $u(a,y) = 0$ gives

$$-a_{11} N^c_{x1} - a_{12} N_{y1} + a_{16} N_{xy1} + \alpha_x \Theta_0 = 0 \qquad (32)$$

which yields u(x,y) = 0. Similarly, enforcing v(x,b) = 0 gives

$$-a_{12}N^c_{x1} - a_{22}N_{y1} + a_{26}N_{xy1} + \alpha_y\Theta_0 = 0 \qquad (33)$$

which yields v(x,y) = 0. Substituting $g_1 = g_3 = 0$ into Eq. (31) gives

$$-a_{16}N^c_{x1} - a_{26}N_{y1} + a_{66}N_{xy1} + \alpha_{xy}\Theta_0 = 0 \qquad (34)$$

The thermally induced stress resultants for this problem are obtained by solving Eqs. (32)-(34) for N^c_{x1}, N_{y1}, and N_{xy1}. The solution is given by

$$N^c_{x1} = (A_{11}\alpha_x + A_{12}\alpha_y + A_{16}\alpha_{xy})\Theta_0 \qquad (35)$$

$$N_{y1} = (A_{12}\alpha_x + A_{22}\alpha_y + A_{26}\alpha_{xy})\Theta_0 \qquad (36)$$

$$N_{xy1} = -(A_{16}\alpha_x + A_{26}\alpha_y + A_{66}\alpha_{xy})\Theta_0 \qquad (37)$$

Equations (35)-(37) define a combined loading state that is induced by restrained thermal expansion and contraction. These equations show that each of the thermally induced mechanical loads depends on all three laminate coefficients of thermal expansion, and that positive values for the stress resultants are possible even for negative values of Θ_0 (uniform cooling) and vice versa. For example, a laminate could have a negative value of α_x and still have a positive value of N^c_{x1} (axial compression). Thus, the signs of Θ_0 and the parenthetical quantities in Eqs. (35)-(37) must be considered in formulating the buckling problem.

The buckling problem is posed by first substituting Eqs. (35)-(37) into Eqs. (10)-(12), respectively, to obtain expressions for the nondimensional stress resultants that can be used to characterize the thermally induced mechanical loads. In particular, the nondimensional stress resultants are expressed in terms of stiffness-weighted laminate thermal-expansion parameters denoted by $\bar{\alpha}_1$, $\bar{\alpha}_2$, and $\bar{\alpha}_3$. These expressions, with the use of Eqs. (14)-(16), are given by

$$n^c_{x1} = \frac{12b^2}{\pi^2 t^2}\bar{\alpha}_1\Theta_0 = L_1\bar{p} \qquad (38)$$

$$n_{y1} = \frac{12b^2}{\pi^2 t^2}\bar{\alpha}_2\Theta_0 = L_2\bar{p} \qquad (39)$$

$$n_{xy1} = \frac{12b^2}{\pi^2 t^2}\bar{\alpha}_3\Theta_0 = L_3\bar{p} \qquad (40)$$

where

$$\bar{\alpha}_1 = \frac{t^2(A_{11}\alpha_x + A_{12}\alpha_y + A_{16}\alpha_{xy})}{12\sqrt{D_{11}D_{22}}} \qquad (41)$$

$$\bar{\alpha}_2 = \frac{t^2(A_{12}\alpha_x + A_{22}\alpha_y + A_{26}\alpha_{xy})}{12D_{22}} \qquad (42)$$

$$\bar{\alpha}_3 = -\frac{t^2(A_{16}\alpha_x + A_{26}\alpha_y + A_{66}\alpha_{xy})}{12(D_{11}D_{22}^3)^{1/4}} \qquad (43)$$

Equations (10)-(12) and (38)-(40) indicate that N^c_{x1}, N_{y1}, and N_{xy1} are positive-valued when $\bar{\alpha}_1$, $\bar{\alpha}_2$, and $\bar{\alpha}_3$ are positive-valued, respectively, and when Θ_0 is positive-valued. Similarly, N^c_{x1}, N_{y1}, and N_{xy1} are negative-valued when $\bar{\alpha}_1$, $\bar{\alpha}_2$, and $\bar{\alpha}_3$ are positive-valued, respectively, and Θ_0 is negative-valued, or when $\bar{\alpha}_1$, $\bar{\alpha}_2$, and $\bar{\alpha}_3$ are negative-valued, respectively, and Θ_0 is positive-valued. Next, Eqs. (38)-(40) are substituted into Eqs. (18)-(20) to obtain the relationships between the mechanical-buckling coefficients, load factors, and the critical temperature Θ^{cr}_0; that is,

$$K_x \equiv (n^c_{x1})_{cr} = \frac{12b^2}{\pi^2 t^2}\bar{\alpha}_1\Theta^{cr}_0 = L_1\bar{p}_{cr} \qquad (44)$$

$$K_y \equiv (n_{y1})_{cr} = \frac{12b^2}{\pi^2 t^2}\bar{\alpha}_2\Theta^{cr}_0 = L_2\bar{p}_{cr} \qquad (45)$$

$$K_s \equiv (n_{xy1})_{cr} = \frac{12b^2}{\pi^2 t^2}\bar{\alpha}_3\Theta^{cr}_0 = L_3\bar{p}_{cr} \qquad (46)$$

where the critical eigenvalue $\bar{p}_{cr} = \bar{p}_{cr}(\beta, \gamma, \delta, L_1, L_2, L_3)$ for a given set of boundary conditions. For an isotropic material, $\bar{\alpha}_3 = 0$ and $\bar{\alpha}_1 = \bar{\alpha}_2 = \alpha(1+\nu)$, where α is the coefficient of thermal expansion and ν is Poisson's ratio of a homogeneous isotropic material.

The next step in posing the buckling problem is to define the load factors L_1, L_2, and L_3 that appear in Eqs. (38)-(40) and (44)-(46). It is important to reiterate that positive, negative, and zero values for $\bar{\alpha}_1\Theta_0$ correspond to positive, negative, and zero values for N^c_{x1}, respectively (see Fig. 2b). Similarly, positive, negative, and zero values for $\bar{\alpha}_2\Theta_0$ correspond to positive, negative, and zero values for N_{y1}, respectively; and positive, negative, and zero values for $\bar{\alpha}_3\Theta_0$ correspond to positive, negative, and zero values for N_{xy1}, respectively. To define the load factors properly, the signs of N^c_{x1}, N_{y1}, and N_{xy1} must be considered. Specifically, the load factors must be defined such that positive values of L_1, L_2, and L_3 correspond to positive values of N^c_{x1}, N_{y1}, and N_{xy1}, respectively. Moreover, both positive and negative val-

ues of Θ_0 must be considered. These requirements lead to six cases that must be considered in formulating the buckling analysis; that is, the cases for which $\alpha_1\Theta_0 > 0$, $\alpha_1\Theta_0 < 0$, $\alpha_1 = 0$ with $\alpha_2\Theta_0 > 0$, $\alpha_1 = 0$ with $\alpha_2\Theta_0 < 0$, $\alpha_1 = \alpha_2 = 0$ with $\alpha_3\Theta_0 > 0$, and $\alpha_1 = \alpha_2 = 0$ with $\alpha_3\Theta_0 < 0$. The buckling analysis for each of these cases is presented subsequently.

For the case when $\alpha_1\Theta_0 > 0$, $N^c_{x1} > 0$ and $L_1 = 1$ is appropriate (axial compression). The values for the other two load factors that are needed to completely define the prebuckling stress state are obtained by dividing Eqs. (19) and (20) by Eq. (18), with $L_1 = 1$, or by dividing Eqs. (39) and (40) by Eq. (38). This step yields

$$L_2 = \frac{N_{y1}}{N^c_{x1}}\left(\frac{D_{11}}{D_{22}}\right)^{1/2} = \frac{\alpha_2}{\alpha_1} = \frac{A_{12}\alpha_x + A_{22}\alpha_y + A_{26}\alpha_{xy}}{A_{11}\alpha_x + A_{12}\alpha_y + A_{16}\alpha_{xy}}\left(\frac{D_{11}}{D_{22}}\right)^{1/2} \quad (47)$$

$$L_3 = \frac{N_{xy1}}{N^c_{x1}}\left(\frac{D_{11}}{D_{22}}\right)^{1/4} = \frac{\alpha_3}{\alpha_1} = -\frac{A_{16}\alpha_x + A_{26}\alpha_y + A_{66}\alpha_{xy}}{A_{11}\alpha_x + A_{12}\alpha_y + A_{16}\alpha_{xy}}\left(\frac{D_{11}}{D_{22}}\right)^{1/4} \quad (48)$$

For an isotropic material, these expressions reduce to $L_2 = 1$ and $L_3 = 0$. With $L_1 = 1$ and L_2 and L_3 defined by Eqs. (47) and (48), the relationship between the critical value of the mechanical loading parameter $\bar{p}_{cr}$ and the critical temperature Θ_0^{cr} is determined by Eq. (44); that is,

$$K_x = \frac{12b^2}{\pi^2 t^2}\alpha_1\Theta_0^{cr} = \bar{p}_{cr} \quad (49)$$

where $\bar{p}_{cr} = \bar{p}_{cr}(\beta, \gamma, \delta, L_1, L_2, L_3)$ for a given set of boundary conditions. It is important to point out that Eq. (49) yields positive and negative values for Θ_0^{cr} for positive and negative values of α_1, respectively. Moreover, it is important to reiterate that the relationship between $\bar{p}_{cr}$ and the corresponding mechanical buckling coefficients K_x, K_y, and K_s is given by Eqs. (49), (45), and (46), respectively.

For the case when $\alpha_1\Theta_0 < 0$, $N^c_{x1} < 0$ and $L_1 = -1$ is appropriate (axial tension). Like for the previous case, the values for the other two load factors that are needed to completely define the prebuckling stress state are obtained by dividing Eqs. (19) and (20) by Eq. (18), but with $L_1 = -1$, or by dividing Eqs. (39) and (40) by Eq. (38). This step yields

$$L_2 = -\frac{N_{y1}}{N^c_{x1}}\left(\frac{D_{11}}{D_{22}}\right)^{1/2} = -\frac{\alpha_2}{\alpha_1} = -\frac{A_{12}\alpha_x + A_{22}\alpha_y + A_{26}\alpha_{xy}}{A_{11}\alpha_x + A_{12}\alpha_y + A_{16}\alpha_{xy}}\left(\frac{D_{11}}{D_{22}}\right)^{1/2} \quad (50)$$

$$L_3 = -\frac{N_{xy1}}{N^c_{x1}}\left(\frac{D_{11}}{D_{22}}\right)^{1/4} = -\frac{\alpha_3}{\alpha_1} = \frac{A_{16}\alpha_x + A_{26}\alpha_y + A_{66}\alpha_{xy}}{A_{11}\alpha_x + A_{12}\alpha_y + A_{16}\alpha_{xy}}\left(\frac{D_{11}}{D_{22}}\right)^{1/4} \quad (51)$$

With $L_1 = -1$ and L_2 and L_3 defined by Eqs. (50) and (51), the relationship between the critical value of the mechanical loading parameter $\bar{p}_{cr}$ and the critical temperature Θ_0^{cr} is again determined by Eq. (44); that is,

$$K_x = \frac{12b^2}{\pi^2 t^2}\alpha_1\Theta_0^{cr} = -\bar{p}_{cr} \quad (52a)$$

In contrast to the previous case, Eq. (52a) yields positive values for Θ_0^{cr} for negative values of α_1, and vice versa. For laminates with $L_3 = 0$ (balanced laminates) and $L_2 \leq 0$ (transverse tension), no destabilizing compression or shear loads are present and buckling cannot occur because the plate is in a state of biaxial tension. In contrast, when $L_3 = 0$ and $L_2 > 0$, a plate is subjected to axial tension and transverse compression loads. Figures 29-31 of Ref. 1 indicate that an infinitely long plate buckles as a wide column for this type of loading, and that the buckling coefficient $K_y = 1$ and 4 for simply supported and clamped plates, respectively. With K_y known, Eqs. (45) and (52a) give

$$K_x = \frac{12b^2}{\pi^2 t^2}\alpha_1\Theta_0^{cr} = -\frac{K_y}{L_2} \quad (52b)$$

For a general symmetric laminate, the possibility exists that $\alpha_1 = 0$, which implies that $N^c_{x1} = 0$. For this case, $L_1 = 0$ is appropriate and the sign of $\alpha_2\Theta_0$ must be considered in defining the nonzero load factors. In particular, for $\alpha_2\Theta_0 > 0$, $N_{y1} > 0$ and $L_1 = 0$ and $L_2 = 1$ are appropriate (transverse compression). The value for the load factor L_3 that is needed to completely define the prebuckling stress state is obtained by dividing Eq. (20) by Eq. (19), with $L_2 = 1$, or by dividing Eqs. (40) by Eq. (39). This step yields

$$L_3 = \frac{N_{xy1}}{N_{y1}}\left(\frac{D_{22}}{D_{11}}\right)^{1/4} = \frac{\alpha_3}{\alpha_2} = -\frac{A_{16}\alpha_x + A_{26}\alpha_y + A_{66}\alpha_{xy}}{A_{12}\alpha_x + A_{22}\alpha_y + A_{26}\alpha_{xy}}\left(\frac{D_{22}}{D_{11}}\right)^{1/4} \quad (53)$$

The relationship between L_3 and the mechanical-buckling coefficients K_y and K_s is shown in Figs. 24-27 of Ref. 1. With $L_1 = 0$, $L_2 = 1$, and L_3 defined by Eq. (53), the relationship between the critical value of the mechanical loading parameter $\bar{p}_{cr}$ and the critical temperature Θ_0^{cr} is determined by Eq. (45); that is,

$$K_y = \frac{12b^2}{\pi^2 t^2}\alpha_2\Theta_0^{cr} = \bar{p}_{cr} \qquad (54a)$$

It is important to point out that Eq. (54a) yields positive and negative values for Θ_0^{cr} for positive and negative values of α_2, respectively. For laminates with $L_3 = 0$ (balanced laminates) a plate is subjected to only transverse compression. Thus, an infinitely long plate buckles as a wide column for this type of loading, and the buckling coefficient $K_y = 1$ and 4 for simply supported and clamped plates, respectively. With K_y known, Eq. (45) gives

$$\frac{12b^2}{\pi^2 t^2}\alpha_2\Theta_0^{cr} = K_y \qquad (54b)$$

For the case when $\alpha_1 = 0$ and $\alpha_2\Theta_0 < 0$, $N_{y1} < 0$ and $L_1 = 0$ and $L_2 = -1$ are appropriate (transverse tension). Like for the previous case, the value for the load factor L_3 that is needed to completely define the prebuckling stress state is obtained by dividing Eq. (20) by Eq. (19), with $L_2 = -1$, or by dividing Eqs. (40) by Eq. (39). This step yields

$$L_3 = -\frac{N_{xy1}}{N_{y1}}\left(\frac{D_{22}}{D_{11}}\right)^{1/4} = -\frac{\alpha_3}{\alpha_2} = \frac{A_{16}\alpha_x + A_{26}\alpha_y + A_{66}\alpha_{xy}}{A_{12}\alpha_x + A_{22}\alpha_y + A_{26}\alpha_{xy}}\left(\frac{D_{22}}{D_{11}}\right)^{1/4} \qquad (55)$$

Like the previous case, the relationship between L_3 and the mechanical-buckling coefficients K_y and K_s is shown in Figs. 24-27 of Ref. 1. With $L_1 = 0$, $L_2 = -1$, and L_3 defined by Eq. (55), the relationship between the critical value of the mechanical loading parameter $\bar{p}_{cr}$ and the critical temperature Θ_0^{cr} is determined by Eq. (45); that is,

$$K_y = \frac{12b^2}{\pi^2 t^2}\alpha_2\Theta_0^{cr} = -\bar{p}_{cr} \qquad (56)$$

For this case, Eq. (56) yields positive values for Θ_0^{cr} for negative values of α_2, and vice versa. For laminates with $L_3 = 0$ (balanced laminates), no destabilizing compression or shear loads are present and buckling cannot occur because the plate is in a state of uniaxial tension.

For the case with $\alpha_1 = \alpha_2 = 0$ and $\alpha_3\Theta_0 > 0$, $N_{x1}^c = N_{y1} = 0$ and $N_{xy1} > 0$, which implies that $L_1 = L_2 = 0$, and that $L_3 = 1$ is appropriate (positive shear loading). With $L_1 = 0$, $L_2 = 0$, and $L_3 = 1$, the relationship between the critical value of the mechanical loading parameter $\bar{p}_{cr}$ and the critical temperature Θ_0^{cr} is determined by Eq. (46); that is,

$$K_s = \frac{12b^2}{\pi^2 t^2}\alpha_3\Theta_0^{cr} = \bar{p}_{cr} \qquad (57)$$

Again, it is important to point out that Eq. (57) yields positive and negative values for Θ_0^{cr} for positive and negative values of α_3, respectively. In addition, values of the mechanical-buckling coefficient K_s for several laminates are given in Ref. 1.

The final case to consider is when $\alpha_1 = \alpha_2 = 0$ and $\alpha_3\Theta_0 < 0$. For this case, $N_{x1}^c = N_{y1} = 0$ and $N_{xy1} < 0$, which implies that $L_1 = L_2 = 0$, and that $L_3 = -1$ is appropriate (negative shear loading). With $L_1 = 0$, $L_2 = 0$, and $L_3 = -1$, the relationship between the critical value of the mechanical loading parameter $\bar{p}_{cr}$ and the critical temperature Θ_0^{cr} is again determined by Eq. (46); that is,

$$K_s = \frac{12b^2}{\pi^2 t^2}\alpha_3\Theta_0^{cr} = -\bar{p}_{cr} \qquad (58)$$

In contrast to the previous case, Eq. (58) yields positive values for Θ_0^{cr} for negative values of α_3, and vice versa.

It is important to mention that the approach used herein to define the prebuckling stress state and the critical temperature Θ_0^{cr} also applies for a more sophisticated plate theory, like a first-order transverse-shear deformation theory. For this theory, $\bar{p}_{cr}$ would depend also upon additional nondimensional parameters that characterize the transverse-shear flexibility. Thus, the only difference in the results for the two plate bending theories is the actual value of $\bar{p}_{cr}$ that is used in Eqs. (44)-(46), for a given problem. It is also important to point out that $\bar{p}_{cr}$ for an infinitely long plate does not depend on the parameter α_{xy}. This fact has been shown in Refs. 1-4.

Results for Common Laminates and Discussion

Results are presented in this section and in Figs. 3-13, that illustrate behavioral trends for several common symmetrically laminated plates that are fully restrained against thermal expansion and contraction and subjected to uniform heating or cooling. In particular, results are presented for several common balanced, symmetric laminates that are made of IM7/5260 graphite-bismaleimide material (see Table 1); that is, $[(\pm 45/0/90)_m]_s$ quasi-isotropic laminates, $[(\pm 45/0_2)_m]_s$ and $[(\pm 45/90_2)_m]_s$ quasi-orthotropic laminates, and $[(\pm\theta)_m]_s$ angle-ply laminates, where a positive value of the lamina fiber angle θ is

shown in Fig. 6. The $[(\pm 45/0_2)_m]_s$ and $[(\pm 45/90_2)_m]_s$ laminates are described as quasi-orthotropic because of the presence of a relatively small amount of flexural anisotropy. Results are also presented for $[\pm\theta/0/90]_s$ laminates with angle plies and for a quasi-isotropic laminate whose principal material-coordinate frame is rotated by an angle θ; that is, $[(\pm 45/0/90) + \theta]_s$. In addition, results are presented for similar unbalanced, symmetric laminates; primarily, $[(+45_2/0/90)_m]_s$, $[(+45_2/0_2)_m]_s$, $[(+45_2/90_2)_m]_s$, $[(+\theta)_{2m}]_s$, and $[+\theta_2/0/90]_s$ laminates that exhibit a significant degree of membrane anisotropy in addition to flexural anisotropy. All of the results are based on classical laminated-plate theory and the nominal ply thickness used in the calculations was 0.005 in.

Results are presented in Figs. 3-4 that show the stiffness-weighted laminate thermal expansion parameter α_1 and load factor ratio α_2/α_1 as a function of the number of laminate plies for several balanced and unbalanced, symmetric laminates. In particular, the black solid lines in the figures are for the $[(\pm 45/0/90)_m]_s$, $[(\pm 45/0_2)_m]_s$, and $[(\pm 45/90_2)_m]_s$ balanced, symmetric laminates and three of the gray dashed lines are for the $[(+45_2/0/90)_m]_s$, $[(+45_2/0_2)_m]_s$, and $[(+45_2/90_2)_m]_s$ unbalanced, symmetric laminates. The difference in these two groups of laminates is the presence of membrane anisotropy that is caused by orienting all the 45-degree plies in the same direction. Results are also presented for $[(\pm 45/10_2)_m]_s$ and $[(\pm 45/30_2)_m]_s$ unbalanced, symmetric laminates with two additional gray dashed lines in Figs. 3-4. Similarly, results are presented in Fig. 5 that show the shear-load-factor ratio α_3/α_1 as a function of the number of laminate plies for the same unbalanced, symmetric laminates. The solid black lines in Fig. 5 are for the $[(+45_2/0/90)_m]_s$, $[(+45_2/0_2)_m]_s$, and $[(+45_2/90_2)_m]_s$ laminates and the dashed gray lines are for the $[(\pm 45/10_2)_m]_s$ and $[(\pm 45/30_2)_m]_s$ laminates. The reason for presenting α_2/α_1 and α_3/α_1 in Figs. 4 and 5, respectively, is because these quantities determine the mechanical-buckling load factors L_2 (see Eqs. (47) and (50)) and L_3 (see Eqs. (48) and (51)), respectively, that are used to determine the critical temperature change when α_1 is nonzero.

The results in Fig. 3 indicate that the values of α_1 are all positive. Thus, these laminates are loaded by axial compression when uniformly heated and by axial tension when uniformly cooled (see Eqs. (38) and (10)). The results also show equal values of α_1 for the $[(\pm 45/0_2)_m]_s$ and $[(+45_2/0_2)_m]_s$ laminates, for the $[(\pm 45/0/90)_m]_s$ and $[(+45_2/0/90)_m]_s$ laminates, and for the $[(\pm 45/90_2)_m]_s$ and $[(+45_2/90_2)_m]_s$ laminates, respectively. The largest values of α_1 are exhibited by the $[(\pm 45/90_2)_m]_s$ and $[(+45_2/90_2)_m]_s$ laminates and the smallest by the $[(\pm 45/0_2)_m]_s$ and $[(+45_2/0_2)_m]_s$ laminates. The results also show, for the most part, relatively small variations in α_1 with the number of laminate plies, with the largest variations exhibited by the $[(\pm 45/0/90)_m]_s$ and $[(+45_2/0/90)_m]_s$ laminates.

The results in Fig. 4 indicate that the values of α_2/α_1 are all positive, which means that the values for α_2 are positive because the values of α_1 are all positive. Thus, the restrained thermal expansion and contraction induces a uniform compressive stress in the y-coordinate direction for uniform heating and a uniform tension stress for uniform cooling (see Eqs. (39) and (11)). The results also show equal values of α_2/α_1 for the $[(\pm 45/0_2)_m]_s$ and $[(+45_2/0_2)_m]_s$ laminates, for the $[(\pm 45/0/90)_m]_s$ and $[(+45_2/0/90)_m]_s$ laminates, and for the $[(\pm 45/90_2)_m]_s$ and $[(+45_2/90_2)_m]_s$ laminates, respectively. The largest values of α_2/α_1 are exhibited by the $[(\pm 45/0_2)_m]_s$ and $[(+45_2/0_2)_m]_s$ laminates ($\alpha_2/\alpha_1 = 3.2$) and the smallest by the $[(\pm 45/90_2)_m]_s$ and $[(+45_2/90_2)_m]_s$ laminates ($\alpha_2/\alpha_1 = 0.28$). The results also show, to a large extent, relatively small variations in α_2/α_1 with the number of laminate plies. However, the results in Fig. 4 also show a substantial, monotonically increasing variation in α_2/α_1 with the number of laminate plies for the $[(\pm 45/0_2)_m]_s$, $[(+45_2/0_2)_m]_s$, and $[(\pm 45/10_2)_m]_s$ laminates.

The results in Fig. 5 also indicate that the values of α_3/α_1 are all positive, which means that the values for α_3 are positive because the values of α_1 are all positive. Thus, the restrained thermal expansion and contraction induces a uniform positive shear stress for uniform heating and a uniform negative shear stress for uniform cooling (see Eqs. (40) and (12)). The results also show nearly equal values of α_3/α_1 for the $[(\pm 45/10_2)_m]_s$ and $[(+45_2/90_2)_m]_s$ laminates for $m > 2$. The largest values of α_3/α_1 are exhibited by the $[(+45_2/0_2)_m]_s$ laminates ($\alpha_3/\alpha_1 = 0.53$) and the smallest by the $[(\pm 45/10_2)_m]_s$ laminates ($\alpha_3/\alpha_1 = 0.15$). The results in Fig. 5 also show relatively small variations in α_3/α_1 with the number of

laminate plies. The largest variation in α_y/α_1 with the number of laminate plies is exhibited by the $[(+45_2/0_2)_m]_s$ laminates.

Three curves are presented in Fig. 6-7 that show the stiffness-weighted laminate thermal-expansion parameter α_1 and load factor ratio α_2/α_1 as a function of the fiber angle, $0^\circ \leq \theta \leq 90^\circ$, for $[(\pm\theta)_m]_s$, $[\pm\theta/0/90]_s$, $[(\pm45/0/90) + \theta]_s$ balanced laminates and for $[(+\theta)_{2m}]_s$ and $[+\theta_2/0/90]_s$ unbalanced laminates. Specifically, the black solid lines in the figures are for the $[(\pm\theta)_m]_s$ and $[(+\theta)_{2m}]_s$ laminates and are independent of the value of the stacking sequence number, m. The dashed lines are for the $[\pm\theta/0/90]_s$ and $[+\theta_2/0/90]_s$ laminates, and the solid gray curves are for the $[(\pm45/0/90) + \theta]_s$ laminates. Likewise, results are presented in Fig. 8 that show the shear-load-factor ratio α_y/α_1 as a function of the fiber angle θ for the $[(+\theta)_{2m}]_s$ and $[+\theta_2/0/90]_s$ unbalanced laminates. In Fig. 8, the solid and dashed black curves are for the $[(+\theta)_{2m}]_s$ and $[+\theta_2/0/90]_s$ laminates, respectively.

The results in Fig. 6 indicate that all of the laminates exhibit $\alpha_1 > 0$, for all values of θ considered. Thus, these laminates are also loaded by axial compression when uniformly heated and by axial tension when uniformly cooled. The largest and smallest values of α_1, and greatest variations, are exhibited by the $[(\pm\theta)_m]_s$ and $[(+\theta)_{2m}]_s$ laminates. Both the $[(\pm\theta)_m]_s$ and $[(+\theta)_{2m}]_s$ and the $[\pm\theta/0/90]_s$ and $[+\theta_2/0/90]_s$ laminates exhibit a monotonic increase in α_1 with increasing values of θ. The values of α_1 for the $[(\pm45/0/90) + \theta]_s$ laminates decrease monotonically with increasing values of θ up to 45° and then increase monotonically. Moreover, the solid gray curve for these laminates is symmetic about the vertical line $\theta = 45^\circ$.

The results in Fig. 7 indicate that the values of α_2/α_1 are all positive, which means that the values for α_2 are positive because the values of α_1 are all positive. Thus, the restrained thermal expansion and contraction induces a uniform transverse compressive stress N_{y1} for uniform heating and a uniform transverse tension stress for uniform cooling. The largest and smallest values of α_2/α_1, and greatest variations, are exhibited by the $[(\pm\theta)_m]_s$ and $[(+\theta)_{2m}]_s$ laminates. Specifically, the largest and smallest values are given by $\alpha_2/\alpha_1 = 14.39$ and 0.07, respectively. Both the $[(\pm\theta)_m]_s$ and $[(+\theta)_{2m}]_s$ and the $[\pm\theta/0/90]_s$ and $[+\theta_2/0/90]_s$ laminates exhibit a monotonic decrease in α_2/α_1 with increasing values of θ, approaching a value of zero. The variation in the values of α_2/α_1 with fiber angle for the $[(\pm45/0/90) + \theta]_s$ laminates is benign compared to the other laminates.

The results in Fig. 8 also indicate that the values of α_y/α_1 are all positive, which means that the values for α_3 are positive because the values of α_1 are all positive. Thus, the restrained thermal expansion and contraction induces a uniform positive shear stress for uniform heating and a uniform negative shear stress for uniform cooling. Overall, the results show that the values of α_y/α_1 are greater for the $[(+\theta)_{2m}]_s$ laminates than for the $[+\theta_2/0/90]_s$ laminates, with respect to the fiber angle θ. In addition, the results show larger variations in α_y/α_1 for both laminates for values of the fiber angle less than approximately 45°. The largest value of α_y/α_1, exhibited by the $[(+\theta)_{2m}]_s$ laminates, is given approximately by $\alpha_y/\alpha_1 = 1.16$ at approximately $\theta = 21^\circ$. The largest value of α_y/α_1 exhibited by the $[+\theta_2/0/90]_s$ laminates is given approximately by $\alpha_y/\alpha_1 = 0.43$ at approximately $\theta = 26^\circ$.

For all of the unbalanced laminates considered in Figs. 3-8, biaxial compression and positive shear loading exists when the laminates are subjected to uniform heating. For uniform cooling, biaxial tension and negative shear loading exists in the laminates. Moreover, a biaxial compression stress state exists in the balanced laminates subjected to uniform heating, and a biaxial tension stress state exists in the balanced laminates subjected to uniform cooling, which means that buckling cannot occur. Furthermore, it was determined that elastic buckling does not occur for the unbalanced laminates considered in Figs. 3-8 that are subjected to uniform cooling.

Results are presented in Figs. 9 and 10 that show the critical temperature change $\frac{12b^2}{\pi^2 t^2}\Theta_0^\sigma$ for uniform heating as a function of the number of laminate plies for the $[(\pm45/0/90)_m]_s$, $[(\pm45/0_2)_m]_s$, and $[(\pm45/90_2)_m]_s$ balanced laminates and the $[(+45_2/0/90)_m]_s$, $[(+45_2/0_2)_m]_s$, $[(+45_2/90_2)_m]_s$, $[(\pm45/10_2)_m]_s$, and

$[(\pm 45/30_2)_m]_s$ unbalanced laminates. Similarly, results are presented in Figs. 11 and 12 that show the critical temperature change for uniform heating as a function of the fiber angle θ for the $[\pm\theta]_s$, $[(+\theta)_{2m}]_s$, and $[(\pm\theta)_m]_s$ $(m > 5)$ laminates, and for the $[\pm\theta/0/90]_s$, $[+\theta_2/0/90]_s$, and $[(\pm 45/0/90) + \theta]_s$ laminates, respectively. The results in Figs. 9 and 10 correspond to results for plates with simply supported and clamped edges, respectively. The results were obtained by computing the ratios α_2/α_1 and α_3/α_1 first. Next, the load factors L_2 and L_3 were determined by using Eqs. (47) and (48), respectively. Then, the critical value of the loading parameter $\bar{p}_{cr}$ was determined for each of the laminates and the critical temperature change was obtained by using Eq. (49). Equations (47)-(49) were used because $\alpha_1\Theta_0 > 0$ for these laminates when subjected to uniform heating. For these laminates, the critical value of the loading parameter depends on the flexural boundary conditions, the plate flexural orthotropy and flexural anisotropy, and the values of the load factors L_2 and L_3, which depend on the stiffness-weighted laminate thermal-expansion parameters. The stiffness-weighted laminate thermal-expansion parameters depend on the plate membrane orthotropy, membrane anisotropy, and the stiffnesses associated with pure bending action.

The results in Figs. 9 and 10 indicate that the critical temperature $\frac{12b^2}{\pi^2 t^2}\Theta_0^{cr}$ is highly dependent on the arrangement of the 45-deg, 0-deg, and 90-deg plies. Generally, as the number of plies increases, the magnitude of the critical temperature change decreases for about half of the laminates and increases for the other half. Overall, the plates with clamped edges are more buckling resistant than the corresponding plates with simply supported edges, as expected. The clamped and simply supported $[(\pm 45/90_2)_m]_s$ laminates require the most heating to cause buckling and the simply supported $[(\pm 45/0_2)_m]_s$, $[(+45_2/0_2)_m]_s$, and $[(\pm 45/10_2)_m]_s$ laminates and the clamped $[(+45_2/0_2)_m]_s$ laminates require the least amount of heating.

The results in Fig. 11 indicate that the critical temperature change $\frac{12b^2}{\pi^2 t^2}\Theta_0^{cr}$ for the $[\pm\theta]_s$, $[(+\theta)_{2m}]_s$, and $[(\pm\theta)_m]_s$ $(m > 5)$ laminates is highly dependent on the fiber angle θ. In particular, the results for the clamped and simply supported $[\pm\theta]_s$ and $[(\pm\theta)_m]_s$ $(m > 5)$ laminates show substantial increase in the critical temperature change with increasing θ for values up to approximately 55° and 62°, respectively, followed by a significant decrease. In addition, the $[(\pm\theta)_m]_s$ $(m > 5)$ laminates require more heating to cause buckling than the corresponding $[\pm\theta]_s$ laminates. The results for the $[(+\theta)_{2m}]_s$ laminates show a monotonic increase in the critical temperature change with θ, but the temperature changes are always less than or equal to those for the corresponding $[\pm\theta]_s$ and $[(\pm\theta)_m]_s$ $(m > 5)$ laminates. Thus, the $[(+\theta)_{2m}]_s$ laminates generally require less heating to cause buckling than the other corresponding laminates shown in Fig. 11. Overall, the plates with clamped edges are much more buckling resistant than the corresponding plates with simply supported edges, as expected.

The results in Fig. 12 indicate that the critical temperature change $\frac{12b^2}{\pi^2 t^2}\Theta_0^{cr}$ for the $[\pm\theta/0/90]_s$, $[+\theta_2/0/90]_s$, and $[(\pm 45/0/90) + \theta]_s$ laminates is also highly dependent on the fiber angle θ. Specifically, the results for the $[\pm\theta/0/90]_s$ laminates exhibit a trend similar to the results for the balanced laminates shown in Fig. 11; that is, the clamped and simply supported $[\pm\theta/0/90]_s$ laminates exhibit a substantial increase in the critical temperature change with increasing θ for values up to approximately 57° and 67°, respectively, followed by a significant decrease. Like the unbalanced laminates of Fig. 11, the results for the $[+\theta_2/0/90]_s$ laminates show a monotonic increase in the critical temperature change with θ, but the temperature changes are always less than or equal to those for the corresponding $[\pm\theta/0/90]_s$ laminates. Thus, the $[+\theta_2/0/90]_s$ laminates require, for the most part, less heating to cause buckling than the corresponding $[\pm\theta/0/90]_s$ laminates. Generally, the $[(\pm 45/0/90) + \theta]_s$ laminates require more uniform heating to cause buckling than the other corresponding laminates shown in Fig. 12, and exhibit greater values of the critical temperature change over a larger range of θ. Moreover, the critical temperature change for the $[(\pm 45/0/90) + \theta]_s$ laminates exhibits the smallest variations with fiber angle for the laminates shown in Fig. 12. Like for the laminates of Fig. 11, the laminates in Fig. 12 with clamped edges are much more buckling resistant than the corresponding plates with simply supported edges, as expected.

The data presented in Figs. 9-12 are given in a compact form and are applicable to an infinite range of plate width-to-thickness ratios, b/t. Once the number of laminate plies is selected, the critical temperature change Θ_0^{cr} can be found as a function of the plate width b for a given laminate family. However, it is important to keep in

mind the limitations of classical laminated-plate bending theory as the plate width-to-thickness ratio b/t becomes smaller than a value of approximately 20. Results of this type are useful in structural design and are shown for the $[(\pm 45/0/90)_m]_s$ quasi-isotropic laminates in Fig. 13. Two sets of curves are shown for various values of the stacking sequence number m in Fig. 13. Moreover, the results are shown for a maximum temperature-change magnitude of 300 °F. This maximum temperature-change magnitude was selected to ensure a regime of heating in which the material behavior is linear. The solid lines in these figures are for plates with simply supported edges and the dashed lines are for plates with clamped edges. As indicated by Eq. (49), the magnitude of Θ_0^{σ} shown in the figure decreases proportionally to the inverse square of the plate width b.

Generic Results and Examples

The simplicity of the equations presented herein that are like Eq. (49) in form suggested that generic buckling design charts, similar to those presented in Refs. 1-5, could be obtained for the thermal buckling problem of the present study. Specifically, generic design data can be obtained from charts that show the stiffness-weighted laminate thermal-expansion parameters α_1, α_2, and α_3; the flexural orthotropy parameter β; and the flexural anisotropy parameters γ and δ as a function of material system and laminate stacking sequence, and from charts that show the critical value of the loading parameter $\bar{p}_{cr}$, or buckling interaction curves, as a function of flexural boundary conditions, β, γ, δ, L_1, L_2 and L_3. Results of this type illustrate the key aspects of the behavior and show overall trends and sensitivity of the behavior to changes in the parameters. Several figures that illustrate the utility of this type of design data are presented subsequently.

Values of the Nondimensional Parameters

Values of the nondimensional parameters that are used herein are presented in this section for $[(\pm 45/0/90)_m]_s$ quasi-isotropic, $[(\pm\theta)_m]_s$ angle-ply, and $[(+\theta)_{2m}]_s$ unidirectional off-axis laminates. Nine different contemporary material systems are used. These material systems include boron-aluminum, S-glass-epoxy, a typical boron-epoxy, AS4/3501-6 graphite-epoxy, AS4/3502 graphite-epoxy, IM7/5260 graphite-bismaleimide, Kevlar 49-epoxy, IM7/PETI-5, and P-100/3502 pitch-epoxy materials. The mechanical properties of these material systems are presented in Table 1 and the nominal ply thickness is 0.005 in.

Parameters for $[(\pm 45/0/90)_m]_s$ laminates. Values of α_1 and α_2/α_1 for $[(\pm 45/0/90)_m]_s$ quasi-isotropic laminates are presented in Figs. 14 and 15, respectively, for the nine material systems. The results show a wide variation in α_1 with material system for the laminate considered. Moreover, α_1 is positive for all the material systems except the P-100/3502 pitch-epoxy material. Similarly, α_2/α_1 is positive for all the material systems and $1 < \alpha_2/\alpha_1 < 1.2$. These values for α_2/α_1 indicate that α_2 is also positive for all the material systems except the P-100/3502 pitch-epoxy material. Thus, the laminates made from all the material systems except the P-100/3502 pitch-epoxy material are loaded by biaxial compression when uniformly heated and by biaxial tension when uniformly cooled, and as a result can buckle only for uniform heating. The laminates made from the P-100/3502 pitch-epoxy material are loaded by biaxial tension when uniformly heated and by biaxial compression when uniformly cooled. These laminates must be cooled to buckle. The results also show that some material systems yield a slightly larger variation in α_1 and α_2/α_1 with the number of laminate plies. Overall, Figs. 14 and 15 show that there is a wide range of possibilities available for tailoring the thermal buckling characteristics of a laminate family.

The remaining parameters needed for a buckling analysis of the long $[(\pm 45/0/90)_m]_s$ quasi-isotropic laminates are the the nondimensional flexural orthotropy parameter β and the flexural anisotropy parameters γ and δ. Values for these parameters are not presented herein. The parameters are given in Ref. 5 as a function of the stacking-sequence number m for the 9 material systems, along with a discussion of their characteristics. The results in Ref. 5 for these parameters show a series of curves that approach $\beta = 1$, $\gamma = 0$, and $\delta = 0$ from above as the number of plies increases. A homogeneous, isotropic material has values of $\beta = 1$, $\gamma = 0$, and $\delta = 0$. Thus, the results for β, γ, and δ in Ref. 5 give, to some extent, a quantitative measure of quasi-isotropy.

Parameters for $[(\pm\theta)_m]_s$ and $[(+\theta)_{2m}]_s$ laminates. Values of α_1, α_2, and α_3 for $[(\pm\theta)_m]_s$ balanced, angle-ply laminates and $[(+\theta)_{2m}]_s$ unbalanced, unidirectional off-axis laminates composed of the 9 material systems are presented in Figs. 16-18, respectively. The values for α_1 and α_2 are identical for both laminates and indepen-

dent of the stacking sequence number m. The results show a very wide variation in α_1, α_2, and α_3 with material system and with fiber angle θ. The largest variations are exhibited by α_2, followed by α_1. Moreover, α_1 and α_2 are positive for all the material systems except the P-100/3502 pitch-epoxy and Kevlar 49-epoxy materials, which are negative for several values of the fiber angle θ. Similarly, α_3 is positive for all the material systems except the S-glass-epoxy and boron-epoxy materials, which are negative for $0° < \theta < 90°$. Thus, depending on the material system and fiber angle, a laminate may be loaded by various combinations of tension, compression, and shear and may buckle when subjected to uniform heating, cooling, or both. Like the results for the quasi-isotropic laminates, the results in Figs. 16-18 show that there is a very wide range of possibilities available for tailoring the thermal buckling characteristics of a laminate family.

Values of the nondimensional orthotropy parameter β and the nondimensional anisotropy parameters γ and δ for the $[(\pm\theta)_m]_s$ laminates made of the same 9 material systems have also been presented in Ref. 5. The values of β in Ref. 5 for the $[(\pm\theta)_m]_s$ laminates are identical to the corresponding results for the $[(+\theta)_{2m}]_s$ unbalanced, unidirectional off-axis laminates and are independent of the stacking-sequence number m. The results in Ref. 5 show a series of curves for β that vary dramatically with the fiber angle θ and the material system. The largest values of, and greatest variations in, β are generally exhibited by the laminates made of the P-100/3502 pitch-epoxy material. In contrast, the smallest values of, and least variations in, β are generally exhibited by the laminates made of the boron-aluminum material. The values of γ and δ for the $[(\pm\theta)_m]_s$ laminates are strongly dependent on the stacking-sequence number m. The results in Ref. 5 for the flexural anisotropy parameters γ and δ are for m = 1, which corresponds to the highest degree of flexural anisotropy for these laminates. The results in Ref. 5 show a large effect of the fiber angle θ and the material system on the degree of flexural anisotropy for the $[\pm\theta]_s$ laminates. Like the parameter β, the largest values of, and greatest variations in, γ and δ are generally exhibited by the laminates made of the P-100/3502 pitch-epoxy material, and the smallest values of, and least variations in, γ and δ are generally exhibited by the laminates made of the boron-aluminum material.

Values of the nondimensional anisotropy parameters γ and δ for the $[(+\theta)_{2m}]_s$ laminates made of the same 9 material systems are presented in Figs. 19 and 20, respectively. The results for these laminates are independent of the stacking sequence number m and exhibit practically the same trends as the results for corresponding $[\pm\theta]_s$ laminates that are given in Ref. 5. The values of γ and δ for the $[(+\theta)_{2m}]_s$ laminates, however, are generally larger than the corresponding values for the $[(\pm\theta)_m]_s$ laminates. This fact is illustrated in Fig. 21 which shows a comparison of results for $[(\pm\theta)_6]_s$, $[\pm\theta]_s$, and $[(+\theta)_{2m}]_s$ laminates made of IM7/5260 graphite-bismaleimide material. The results in this figure indicate that the $[(+\theta)_{2m}]_s$ unidirectional off-axis and $[\pm\theta]_s$ laminates exhibit similar variations with θ, but the $[(+\theta)_{2m}]_s$ laminates exhibit a substantially higher degree of flexural anisotropy. In addition, the results for the $[(\pm\theta)_6]_s$ laminates indicate that the flexural anisotropy is negligible compared to that of the other laminates.

Buckling Coefficients and Critical Temperature Change

The values of the nondimensional parameters β, γ and δ given in Ref. 5 and presented in the present paper, or from similar figures for other laminates, can be used to determine the buckling coefficients for plates subjected to uniform, combined mechanical loads. More specifically, the critical loading parameter $\bar{p}_{cr}$ and the buckling coefficient K_x, K_y, and K_s depend on the parameters β, γ, and δ for classical laminated-plate theory (see Ref. 1) and the load factors L_1, L_2, and L_3 that define the relative proportions of the inplane loads. For plates subjected to restained thermal expansion and contraction and uniform heating or cooling, the relative proportions of the inplane loads that are induced by the restrained deformation are defined by the stiffness-weighted laminate thermal-expansion parameters α_1, α_2, and α_3 (e.g., see Eqs. (47) and (48)). Thus, generic buckling design charts for plates subjected to mechanical loads can be used directly to obtain critical temperature changes for the thermal buckling problem considered herein, and can be applied to a vast range of laminate constructions that include hybrid laminates made of several materials. Several of these generic buckling design charts that are applicable to balanced and unbalanced, symmetric laminates are presented subsequently.

Charts for balanced laminates. Balanced laminates that are subjected to uniform heating or cooling and fully restrained against thermal expansion and contraction develop, at most, a biaxial stress state ($\alpha_3 = 0$). For the case when α_1 and α_2 are both positive valued, a laminate is loaded by uniform biaxial compression when heated uniformly. In contrast, for the case when $\alpha_1 > 0$ and $\alpha_2 < 0$, a laminate is loaded by uniform axial compression and

transverse tension ($N_{y1} < 0$) when heated uniformly. A similar stress state exist when when $\alpha_1 < 0$ and $\alpha_2 > 0$ and the laminate is uniformly cooled. However, for all three of these loading conditions; $L_1 = 1$, $L_3 = 0$, and L_2 is given by Eq. (47). The critical temperature change $\frac{12b^2}{\pi^2 t^2}\Theta_0^{cr}$ is obtained by dividing both sides of Eq. (49) by α_1, once $\bar{p}_{cr}(\beta, \gamma, \delta, L_1, L_2, L_3)$ is known. The appropriate value for $\bar{p}_{cr}$ is obtained from generic buckling design charts by noting that Eqs. (44) and (45) give $K_x = \bar{p}_{cr}$ and $K_y = L_2\bar{p}_{cr}$, respectively, and that $L_2 = K_y/K_x$. Thus, the critical value of the loading parameter for balanced laminates can be obtained from traditional K_x-K_y buckling interaction curves that are given as a function of the nondimensional parameters β, γ, δ, and the boundary conditions.

For the case when α_1 and α_2 are both positive valued and the laminate is subjected to uniform cooling, or the case when α_1 and α_2 are both negative valued and the laminate is subjected to uniform heating, a state of biaxial tension exists in the laminate. For this loading condition, elastic buckling is not possible. For the case when $\alpha_1 > 0$ and $\alpha_2 < 0$, a laminate is loaded by uniform axial tension and transverse compression when cooled uniformly. A similar stress state exist when when $\alpha_1 < 0$ and $\alpha_2 > 0$ and the laminate is uniformly heated. For both of these cases; $L_1 = -1$, $L_3 = 0$, and L_2 is given by Eq. (50). More importantly, because the only destabilizing load is a transverse compression load, a wide-column buckling mode is the only possibility. Thus, the critical temperature change $\frac{12b^2}{\pi^2 t^2}\Theta_0^{cr}$ is obtained by dividing both sides of Eq. (52b) by α_1. For this special case, $K_y = 1$ and $K_y = 4$ for simply supported and clamped plates, respectively, and $K_x = -K_y/L_2$.

For the case when $\alpha_1 = 0$ and $\alpha_2 < 0$, a laminate is loaded by uniform transverse tension when heated uniformly. A similar stress state exist when when $\alpha_1 = 0$ and $\alpha_2 > 0$ and the laminate is uniformly cooled. For this loading condition, elastic buckling is also not possible. For the cases where $\alpha_1 = 0$ and $\alpha_2 < 0$ and the laminate is cooled uniformly, and where $\alpha_1 = 0$ and $\alpha_2 > 0$ and the laminate is heated uniformly, a state of transverse compression exists. A wide-column buckling mode is the only possibility. The critical temperature change $\frac{12b^2}{\pi^2 t^2}\Theta_0^{cr}$ is obtained by dividing both sides of Eq. (54b) by α_2. For this special case, $K_y = 1$ and $K_y = 4$ for simply supported and clamped plates, respectively.

Examples of traditional K_x-K_y buckling interaction curves that can be used to obtain $\bar{p}_{cr}(\beta, \gamma, \delta, L_1, L_2, L_3)$ described in the previous paragraphs are presented in Fig. 22 for specially orthotropic plates, that have negligible flexural anisotropy ($\gamma = \delta = 0$). In particular, two sets of generic buckling curves are shown in Fig. 22 for plates that are subjected to combined axial compression and transverse tension or compression loads. Results are shown in the figure for six values of the orthotropy parameter β that cover a very wide range of laminate constructions. The solid and dashed curves correspond to results for clamped and simply supported plates, respectively, and the curves for $\beta = 1$ correspond to results for isotropic plates. Similar curves that show the effects of flexural anisotropy are presented in Ref. 1, along with a discussion of the behavioral characteristics. For the K_x-K_y buckling interaction curves shown in Fig. 22, the load factor L_2 appears implicitly as the slope of a line emanating from the origin of the graph. The buckling coefficients that correspond to a given value of L_2 are determined by the point of intersection of the line and the appropriate buckling interaction curve. These points of intersection are depicted in Fig. 22 for the simply supported and clamped plates by the open and filled circular symbols, respectively. Points of intersection that occur on the horizontal portion of the curves, given by $K_y = 1$ and 4 for the simply supported and clamped plates, respectively, correspond to wide-column buckling modes. Similarly, results for negative values of K_x, although not shown in Fig. 22, correspond horizontal extrapolations of the lines $K_y = 1$ and 4, and also correspond to wide-column buckling modes. With the value of L_2 determined from Eq. (47), unique values of K_x and K_y are determined from a figure like Fig. 22, where $\bar{p}_{cr} = K_x$.

Results that are directly analogous to those presented in Fig. 22 are presented in Figs. 23 and 24 in which the buckling coefficient K_x, or equivalently $\bar{p}_{cr}$, is given explicitly in terms of the load factor L_2. An interesting characteristic of Fig. 23 is that the family of curves for the simply supported plates (dashed) and the clamped plates (solid) terminate at points on the gray, solid curves given by $K_x = \frac{1}{L_2}$ and $K_x = \frac{4}{L_2}$, respectively. The curves $K_x = \frac{1}{L_2}$ and $K_x = \frac{4}{L_2}$ correspond to the horizontal portion of the curves in Fig. 22 that are given by $K_y =$

1 and $K_y = 4$ for the simply supported plates (dashed) and the clamped plates (solid), respectively, and represent the wide-column buckling modes. Like in Fig. 22, negative values of K_x (not shown) correspond to wide-column buckling modes.

Typically, when studying the behavior of plates that possesses flexural anisotropy, one likes to know the importance of the anisotropy. Generic curves for simply supported plates that can be used in conjunction with Figs. 23 and 24 to obtain this information are presented in Figs. 25 and 26. The curves indicate the effects of plate flexural anisotropy on the ratio of the buckling coefficients that include and neglect this anisotropy, respectively, as a function of β and L_2. Buckling coefficients that correspond to the neglection of flexural anisotropy are denoted by $K_x|_{\gamma=\delta=0}$. Six groups of curves are shown in each figure that correspond to equal values of the flexural anisotropy parameters. Moreover, three curves are contained in each group that correspond to different values of L_2.

Charts for unbalanced laminates. Unbalanced laminates that are subjected to uniform heating or cooling and fully restrained against thermal expansion and contraction can generally develop a prebuckling stress state that consists of combinations of axial tension or compression, transverse tension or compression, and positive or negative shear. The specific form of the prebuckling stress state is determined by the values of the parameters α_1, α_2, and α_3; which determine the values of the load factors L_1, L_2, and L_3. The specific values of L_1, L_2, and L_3 are obtained by following the same logic presented previously for the balanced laminates and discussed during the presentation of Eqs. (47)-(58). Once L_1, L_2, and L_3 are determined, $\bar{p}_{cr}(\beta, \gamma, \delta, L_1, L_2, L_3)$ can be determined from generic results that give either $\bar{p}_{cr}$ or K_x-K_y-K_s buckling interaction surfaces (or level curves) as a function of L_1, L_2, L_3, β, γ, δ, and the boundary conditions. Then, the critical temperature change $\frac{12b^2}{\pi^2 t^2}\Theta_0^{cr}$ is determined by using the appropriate one of Eqs. (49), (52a), (54a), (56), (57), and (58).

Examples of generic buckling curves are shown in Fig. 27 for plates with negligible flexural anisotropy ($\gamma = \delta = 0$) and subjected to combined axial compression, transverse tension or compression, and shear. These results are applicable to unbalanced, symmetric laminates with negligible flexural anisotropy that develop biaxial and shear loads when restrained from thermal expansion and contraction and can be used to obtain $\bar{p}_{cr}$ described in the previous paragraph. The results shown in Fig. 27 represent the traditional buckling interaction curves and are for a value of $\beta = 1$, which corresponds to results for isotropic plates. The load factors L_2 and L_3 are included in the results in an implicit manner. The solid and dashed curves correspond to results for clamped and simply supported plates, respectively, and are level curves of the corresponding K_x-K_y-K_s buckling interaction surface. Each curve in the figure corresponds to a different magnitude of the shear loading. Moreover, positive and negative values of the shear-buckling coefficient K_s correspond to positive (see Fig. 2b) and negative directions of the shear loading. The buckling coefficients that correspond to given values of the load factors L_2 and L_3 are determined by the point of intersection of the line emanating from the origin of the graph and the appropriate buckling interaction curve. These points of intersection are depicted in Fig. 27 for the simply supported and clamped plates by the open and filled circular symbols, respectively. Points of intersection that occur on the horizontal portion of the curves, given by $K_y = 1$ and 4 for the simply supported and clamped plates, respectively, correspond to wide-column buckling modes. With the values of L_1, L_2, and L_3 determined from the values of the parameters α_1, α_2, and α_3, unique values of K_x, K_y, and K_s are determined from a figure like Fig. 27, and $\bar{p}_{cr}$ is determined from Eqs. (44)-(46). It is worth mentioning that very few results of this type are available in the technical literature.

Results that are directly analogous to those presented in Fig. 27 are presented in Figs. 28-33 for simply supported plates in which the buckling coefficient K_x, or equivalently $\bar{p}_{cr}$, is given explicitly in terms of the load factors L_2 and L_3, with $L_1 = 1$. Thus, the results in these figures are applicable to plates for which the axial load is a compression load. More precisely, K_x is given as a function of L_2 for selected values of L_3, and three different curves are shown in each figure that correspond to different values of β. The curves in Fig. 28 and 29 are for specially orthotropic plates ($\gamma = \delta = 0$) with values of $\beta = 0.5$, 1, and 1.5 and with values of $\beta = 2$, 2.5, and 3, respectively. Curves are given in these figures that apply to both positive and negative shear loads. Similarly, the curves in Figs. 30 and 31, and in Figs. 32 and 33, are for plates with $\gamma = \delta = 0.2$ (slight anisotropy) and $\gamma = \delta = 0.6$ (substantial anisotropy), respectively, and for $\beta = 2$, 2.5, and 3. Moreover, the results in Figs. 30 and 32 are primarily for positive shear loads, and those in Figs. 31 and 33 are for negative shear loads. The distinction between positive and negative shear loads, and the differences in the corresponding results, is caused by the presence of

flexural anisotropy. In each of Figs. 28-33, the curves terminate at points on the gray, solid curves given by $K_x = \frac{1}{L_2}$, which represent the wide-column buckling modes.

Examples

To illustrate the use of the generic figures that have been presented herein, first consider a simply supported $[(\pm 45/90_2)_8]_s$ laminate made of IM7/5260 graphite-bismaleimide material. From a laminate analysis code, or a set of charts like those shown in Figs. 14-21, one could get $\beta = 1.3$, $\gamma = \delta \approx 0$, $\alpha_1 = 2.27 \times 10^{-6}$ /°F, $\alpha_2 = 0.71 \times 10^{-6}$ /°F, and $\alpha_3 = 0$. For this laminate, the only destabilizing loads are biaxial compression loads that are obtained for uniform heating. For this case, $L_1 = 1$, $L_3 = 0$, and $L_2 = 0.27$ is obtained from Eq. (47). For $L_1 = 1$, $K_x = \bar{p}_{cr}$. The value of K_x is obtained from Fig. 23 by interpolating the results in the figure for $\beta = 1$ and $\beta = 1.5$. For $\beta = 1$ and $L_2 = 0.27$, Fig. 23 gives $K_x = 2.9$. Similarly, for $\beta = 1.5$ and $L_2 = 0.27$, Fig. 23 gives $K_x = 3.5$. Interpolating these values gives $K_x = 3.3$ for $\beta = 1.3$. Substituting $K_x = 3.3$ for $\bar{p}_{cr}$ and $\alpha_1 = 2.27 \times 10^{-6}$ /°F into Eq. (49) gives $\frac{12b^2}{\pi^2 t^2}\Theta_0^{cr} = 1.45 \times 10^6$ °F. Next, let the plate width be given by b = 32 in. such that the plate width-to-thickness ratio is b/t = 100. For this plate, $\Theta_0^{cr} \approx 119$°F.

Next, consider a simply supported $[\pm 45/90_2]_s$ laminate made of IM7/5260 graphite-bismaleimide material. From a laminate analysis code, or a set of charts like those shown in Figs. 14-21, one could get $\beta = 2$, $\gamma = \delta \approx 0.2$, $\alpha_1 = 2.39 \times 10^{-6}$ /°F, $\alpha_2 = 1.11 \times 10^{-6}$ /°F, and $\alpha_3 = 0$. For this laminate, the only destabilizing loads are also biaxial compression loads that are obtained for uniform heating. Thus, for this case, $L_1 = 1$, $L_3 = 0$, and $L_2 = 0.47$ is obtained from Eq. (47). Again, for $L_1 = 1$, $K_x = \bar{p}_{cr}$. The value of K_x is obtained directly from Fig. 30 and is given by $K_x = 2.1$, which corresponds to a wide-column buckling mode. Substituting $K_x = 2.1$ for $\bar{p}_{cr}$ and $\alpha_1 = 2.39 \times 10^{-6}$ /°F into Eq. (49) gives $\frac{12b^2}{\pi^2 t^2}\Theta_0^{cr} = 0.88 \times 10^6$ °F. Next, let the plate width be given such that the plate width-to-thickness ratio is b/t = 100. For this plate, $\Theta_0^{cr} \approx 72$°F.

Finally, consider a simply supported $[(+45_2/90_2)_8]_s$ unbalanced laminate made of IM7/5260 graphite-bismaleimide material. From a laminate analysis code, or a set of charts like those shown in Figs. 14-21, one could get $\beta = 1.3$, $\gamma = 0.5$, $\delta = 0.3$, $\alpha_1 = 2.27 \times 10^{-6}$ /°F, $\alpha_2 = 0.71 \times 10^{-6}$ /°F, and $\alpha_3 = 0.38 \times 10^{-6}$ /°F. For this laminate, a state of biaxial compression and positive shear loads arise for uniform heating. Thus, for this case, $L_1 = 1$, $L_2 = 0.27$ is obtained from Eq. (47), and $L_3 = 0.17$ is obtained from Eq. (48). Again, for $L_1 = 1$, $K_x = \bar{p}_{cr}$. From a set of charts like the ones presented herein, one could get $K_x = \bar{p}_{cr} = 2.6$. Substituting $K_x = 2.6$ for $\bar{p}_{cr}$ and $\alpha_1 = 2.27 \times 10^{-6}$ /°F into Eq. (49) gives $\frac{12b^2}{\pi^2 t^2}\Theta_0^{cr} = 1.15 \times 10^6$ °F. Next, let the plate width be given such that the plate width-to-thickness ratio is b/t = 100. For this plate, $\Theta_0^{cr} \approx 95$°F. Comparing this result with the result for the corresponding $[(\pm 45/90_2)_8]_s$ laminate discussed previously shows that the unbalanced laminate is less buckling resistant, as expected because of its higher degree of anisotropy and the presence of a shear load. For the case of uniform cooling, biaxial tension and negative shear loads are induced by the restrained deformation. The load factors for this case are obtained from Eqs. (50) and (51), where $L_1 = -1$. These equations yield $L_2 = -0.27$ and $L_3 = -0.17$. Examination of the load factors indicates that the axial and transverse tension loads are approximately 6 and 1.6 times the magnitude of the destabilizing shear load. For this loading condition, the tension loads are dominant and elastic buckling is not possible.

Concluding Remarks

An analytical approach for synthesizing buckling results and behavior for long, balanced and unbalanced symmetric laminates that are subjected to uniform heating or cooling, and fully restrained thermal expansion and contraction has been presented. A nondimensional buckling analysis for long flexurally anisotropic plates that are subjected to combined loads has been described and useful nondimensional parameters have been presented. In particular, stiffness-weighted thermal-expansion parameters have been presented that can be used to determine critical temperatures, for a wide range of laminate constructions, in terms of physically intuitive, well-known mechanical buckling coefficients. Moreover, the effects of membrane orthotropy and membrane anisotropy on the mechanical, thermally induced prebuckling stress state have been determined.

A large number of results have been presented herein for some common laminates that are intended, to some extent, to facilitate a structural designer's transition to the use of the generic buckling design curves that are

included in the paper. Many of the results were previously unknown. In addition, several results have been presented that show the effect of laminate construction on the buckling behavior, and several cases are presented that indicate when a laminate will buckle because of uniform cooling. Results of this type could be important in the design of vehicles that use liquid fuels. Generic buckling design curves have also been presented that provide physical insight into the buckling problem of the present paper in addition to providing useful design data. In addition, examples have been presented that demonstrate the use of the generic design curves. Overall, the analysis approach and generic results that have been presented indicate the effects or characteristics of laminate thermal expansion, membrane orthotropy and anisotropy, and flexural orthotropy and anisotropy on laminated-plate buckling in a very general and unifying manner. Although the results are based on classical laminated-plate theory and have been demonstrated for infinitely long plates, the approach is applicable to more sophisticated plate theories that incorporate effects such as transverse-shear flexibility and can be used for finite-length plates.

References

[1]Nemeth, M. P., "Buckling Behavior of Long Symmetrically Laminated Plates Subjected to Combined Loadings," NASA TP 3195, May 1992

[2]Nemeth, M. P., "Buckling Behavior of Long Symmetrically Laminated Plates Subjected to Compression, Shear, and Inplane Bending Loads," *AIAA Journal*, Vol. 30, No. 12, December 1992, pp. 2959-2965.

[3]Nemeth, M. P., "Buckling Behavior of Long Anistropic Plates Subjected to Combined Loads," NASA TP 3568, November 1995.

[4] Nemeth, M. P., "Buckling Behavior of Long Symmetrically Laminated Plates Subjected to Shear and Linearly Varying Axial Edge Loads," NASA TP 3659, July 1997.

[5] Nemeth, M. P., "Buckling Behavior of Long Anisotropic Plates Subjected to Restrained Thermal Expansion and Mechanical Loads," *Journal of Thermal Stresses*, Vol. 23, 2000, pp. 873-916.

[6]Nemeth, M. P., "Importance of Anisotropy on Buckling of Compression-Loaded Symmetric Composite Plates," AIAA Journal, Vol. 24, No. 11, November 1986, pp. 1831-1835.

[7]Whitney, J. M., *Structural Analysis of Laminated Anisotropic Plates*, Technomic Publishing Co., Inc., Lancaster, Pennsylvania, 1987.

[8] Hyer, M. W., *Stress Analysis of Fiber-Reinforced Composite Materials*, WCB/McGraw Hill Publishing Co., Inc., Boston, 1998.

Table 1: Lamina properties.

Lamina property*	Material Systems								
	Boron-Al	S-glass-epoxy	Kevlar 49-epoxy	IM7/5260	AS4/3502	AS4/3501-6	Boron-epoxy	IM7/PETI-5	P-100/3502
E_L, Msi	33	7.5	11.02	22.1	18.5	20.01	29.58	20.35	53.5
E_T, Msi	21	1.7	0.8	1.457	1.64	1.30	2.68	1.16	0.73
ν_{LT}	0.23	0.25	0.34	0.258	0.30	0.30	0.23	0.29	0.31
G_{LT}, Msi	7.0	0.80	0.33	0.860	0.87	1.03	0.81	0.61	0.76
α_L x 10⁶/°F	3.2	3.5	-2.22	0.0125	0.25	-0.167	3.38	-0.14	-0.64
α_T x 10⁶/°F	11.0	11.0	43.89	14.91	16.2	15.6	16.83	16.85	17.2

* The subscripts L and T denote the longitudinal (fiber) and transverse (matrix) directions of a specially orthotropic lamina, respectively.

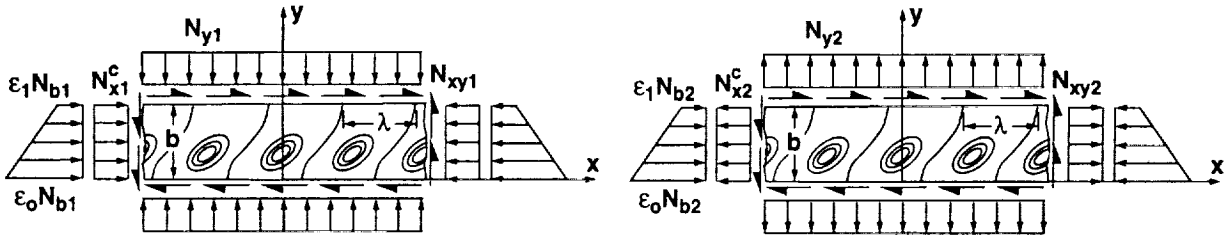

(a) Destabilizing loading system (b) Subcritical loading system

Fig. 1 Sign convention for positive-valued stress resultants.

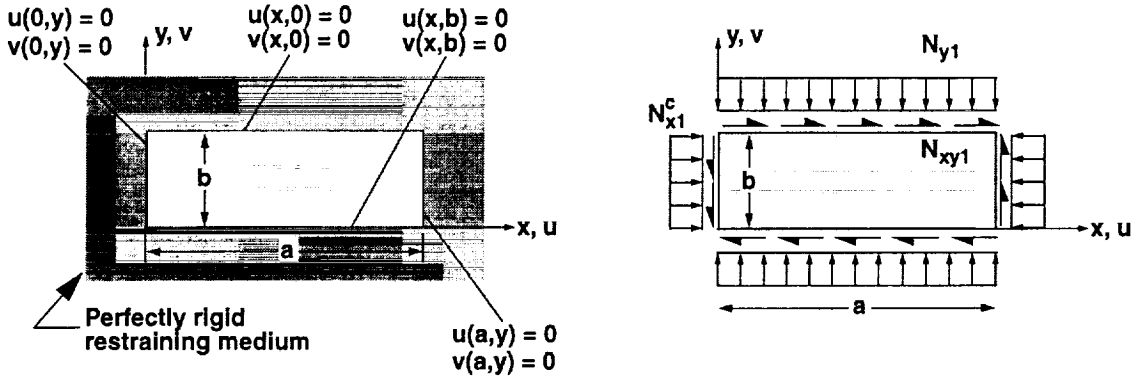

(a) Boundary conditions (b) Positive values for equivalent mechanical loads

Fig. 2 Mechanical loads in a plate fully restrained against axial thermal expansion or contraction caused by uniform heating or cooling.

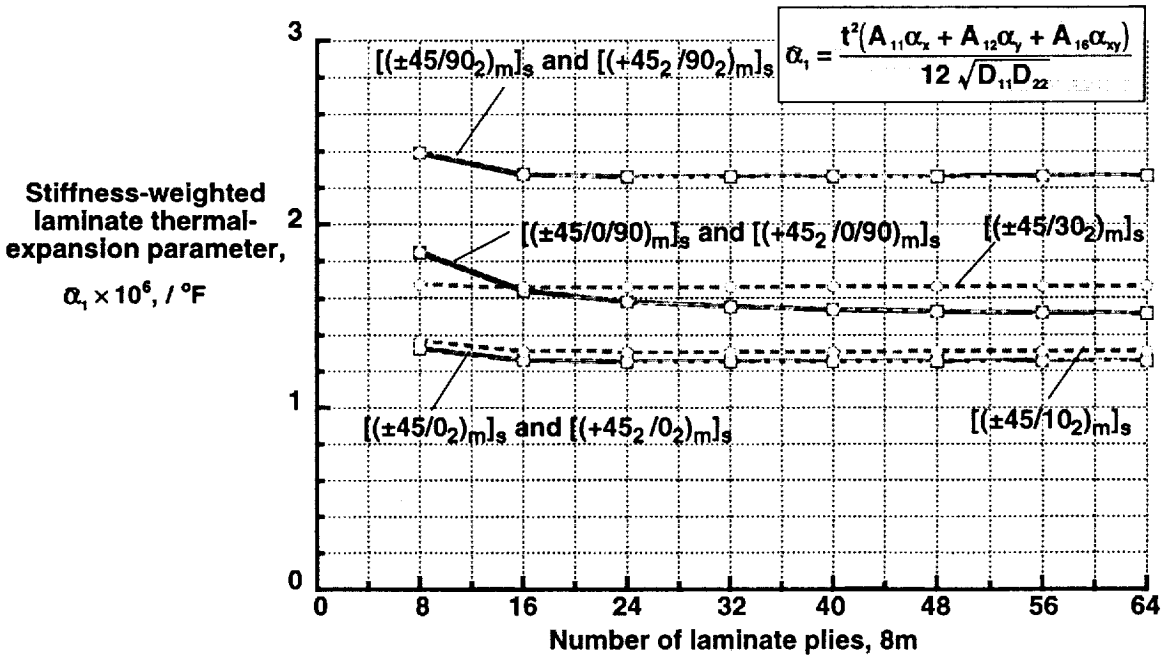

Fig. 3 Stiffness-weighted laminate thermal-expansion parameter $\bar{\alpha}_1$ for laminates made of IM7/5260 material.

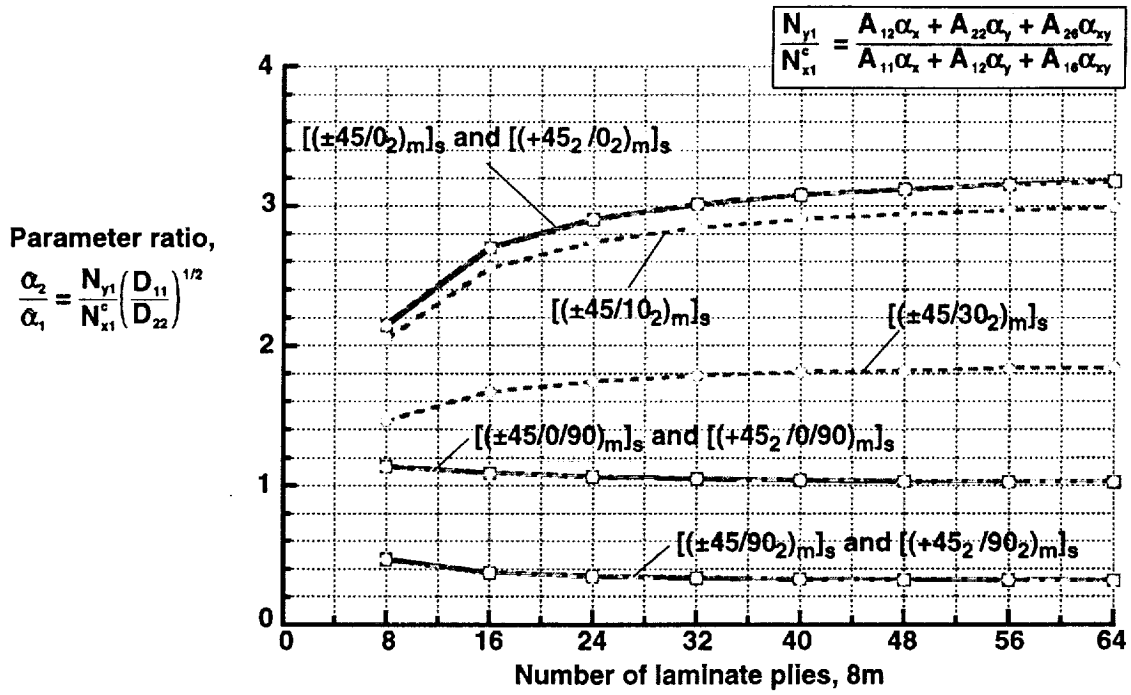

Fig. 4 Ratio of stiffness-weighted thermal-expansion parameters α_1 and α_2 for laminates made of IM7/5260 material.

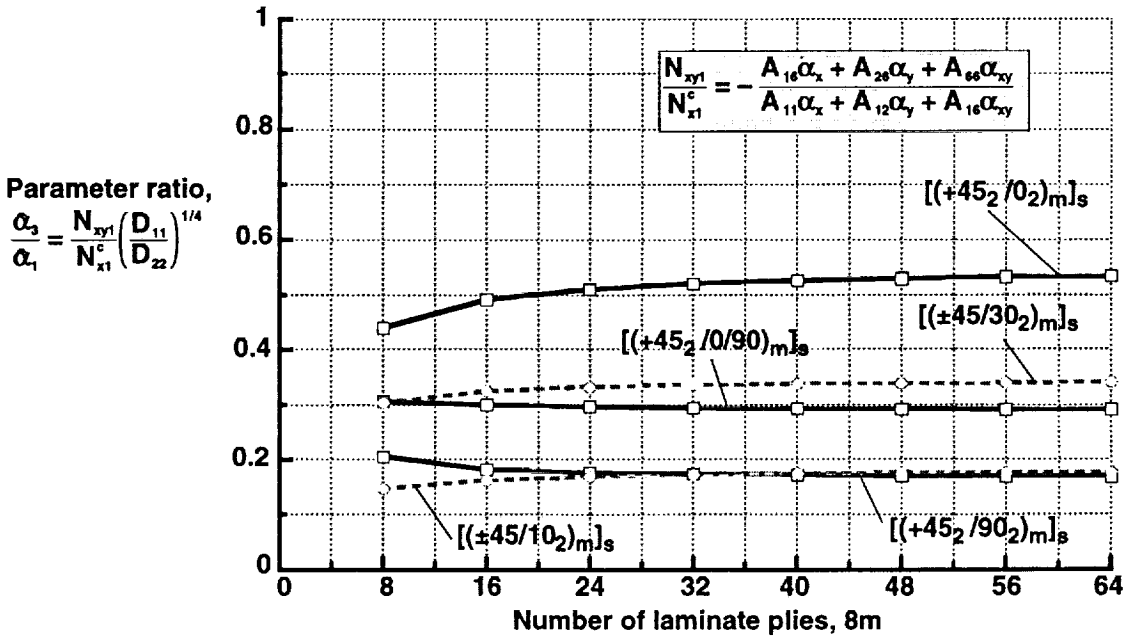

Fig. 5 Ratio of stiffness-weighted thermal-expansion parameters α_1 and α_3 for laminates made of IM7/5260 material.

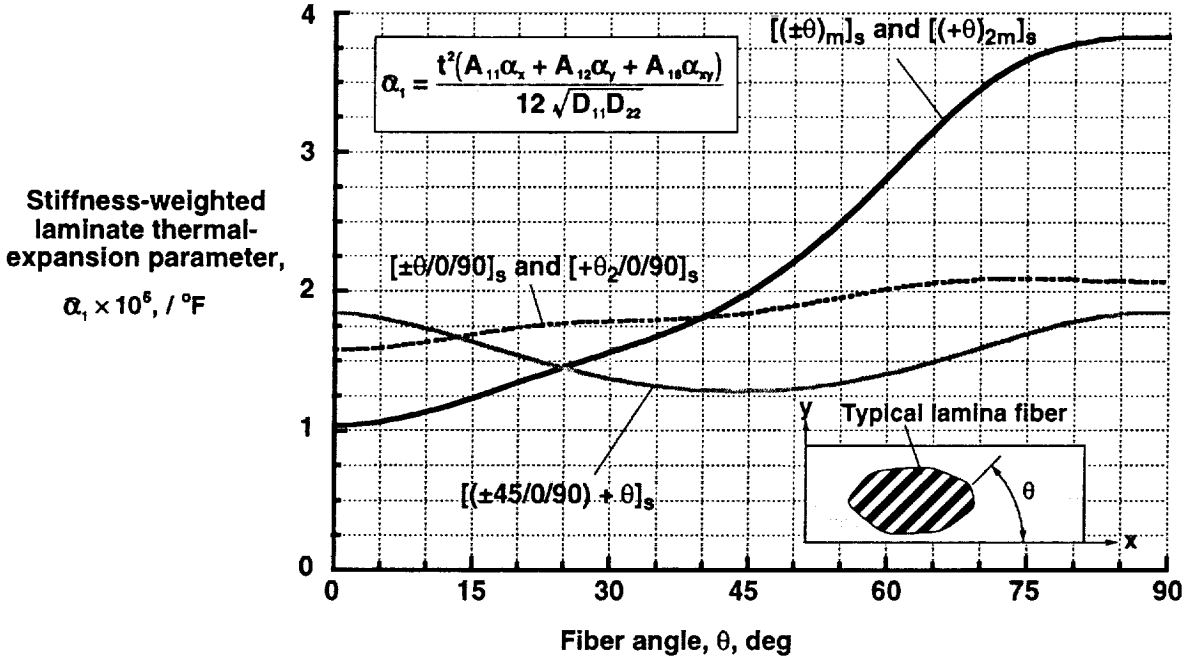

Fig. 6 Stiffness-weighted laminate thermal-expansion parameter $\bar{\alpha}_1$ for balanced and unbalanced laminates with angle-plies and unbalanced, unidirectional off-axis laminates made of IM7/5260 material (m = 1, 2, ...).

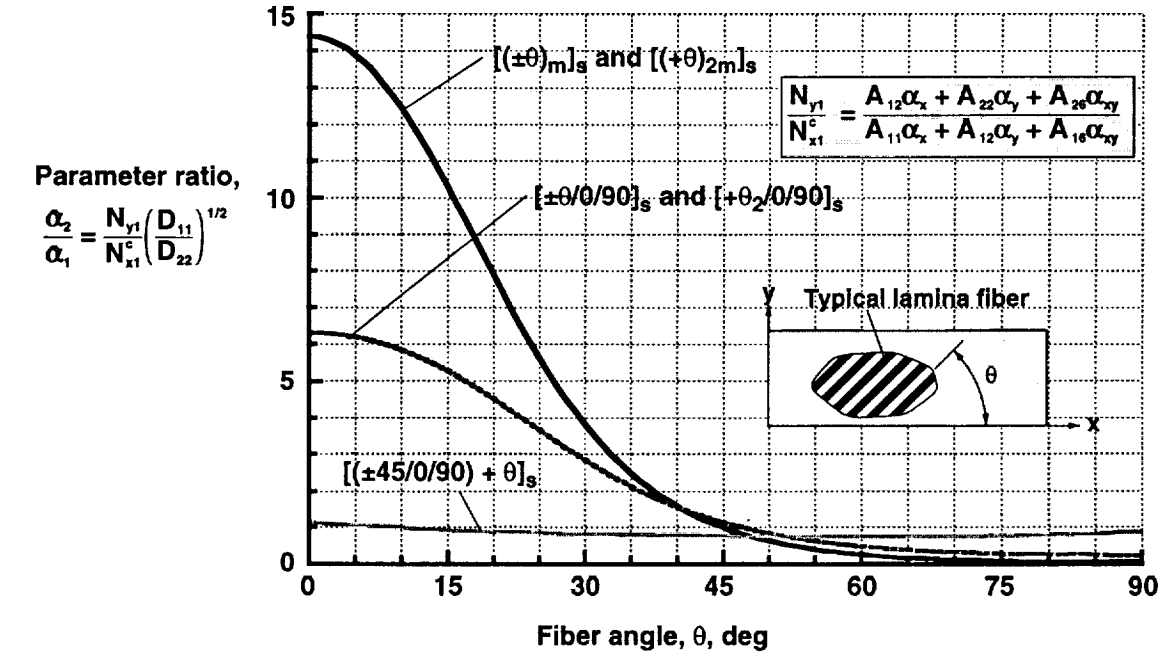

Fig. 7 Ratio of stiffness-weighted thermal-expansion parameters $\bar{\alpha}_1$ and $\bar{\alpha}_2$ for balanced and unbalanced laminates with angle-plies and unbalanced, unidirectional off-axis laminates made of IM7/5260 material (m = 1, 2, ...).

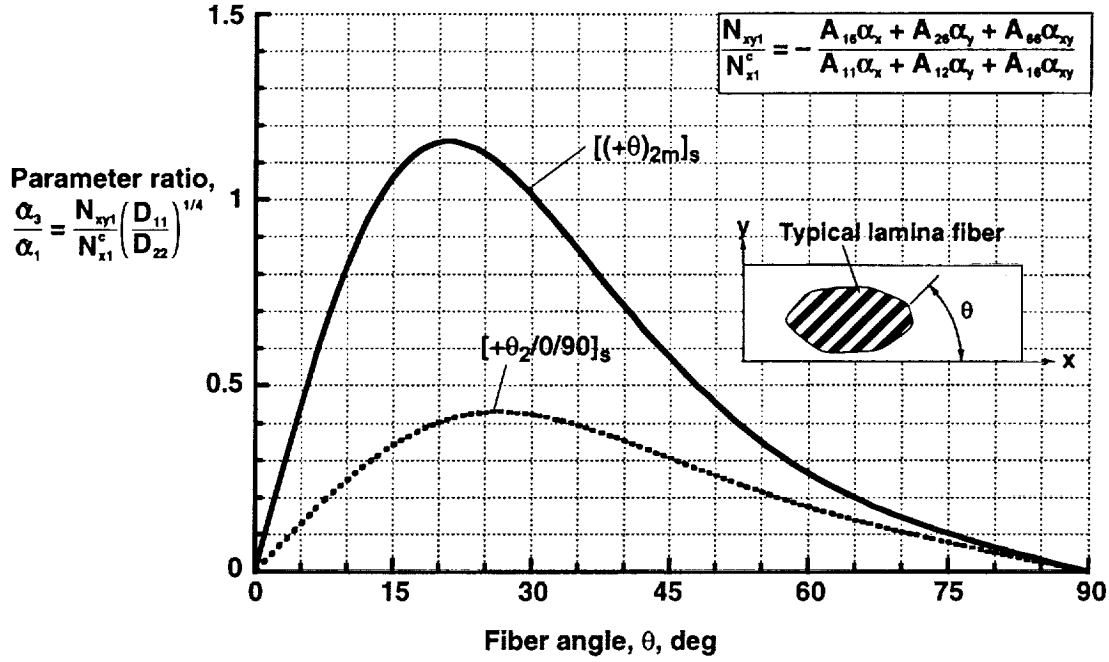

Fig. 8 Ratio of stiffness-weighted thermal-expansion parameters α_1 and α_3 for $[(+\theta)_{2m}]_s$ and $[+\theta_{2z}/0/90]_s$ unbalanced, unidirectional off-axis laminates made of IM7/5260 material (m = 1, 2, ...).

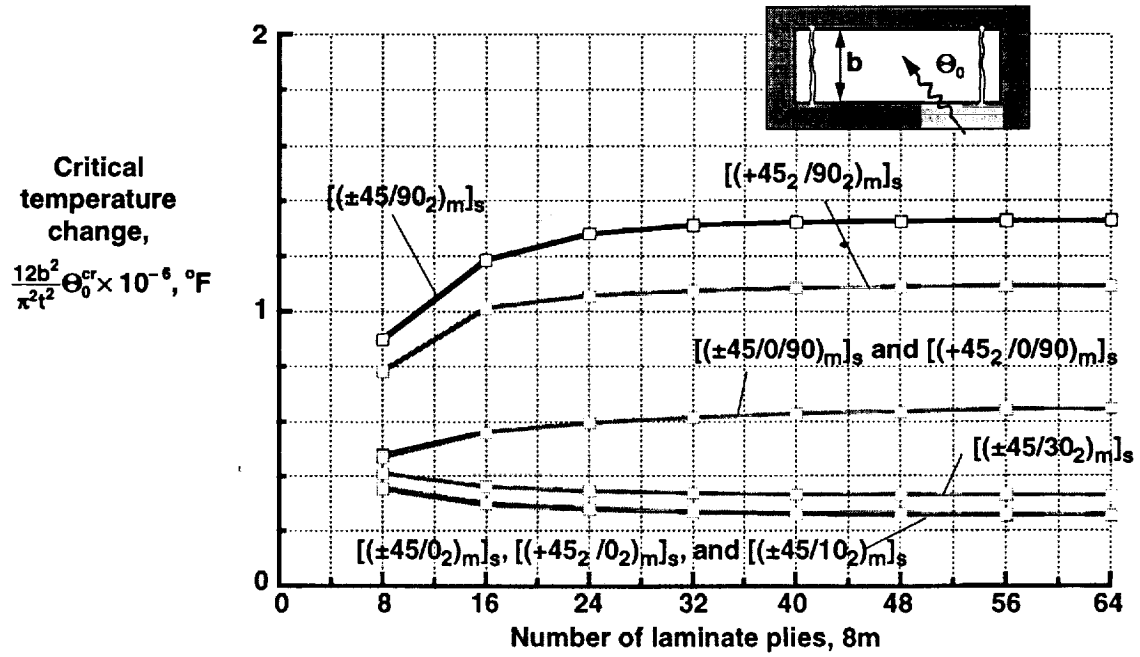

Fig. 9 Critical temperature change for simply supported laminates made of IM7/5260 material, fully restrained against thermal expansion and contraction, and subjected to uniform heating.

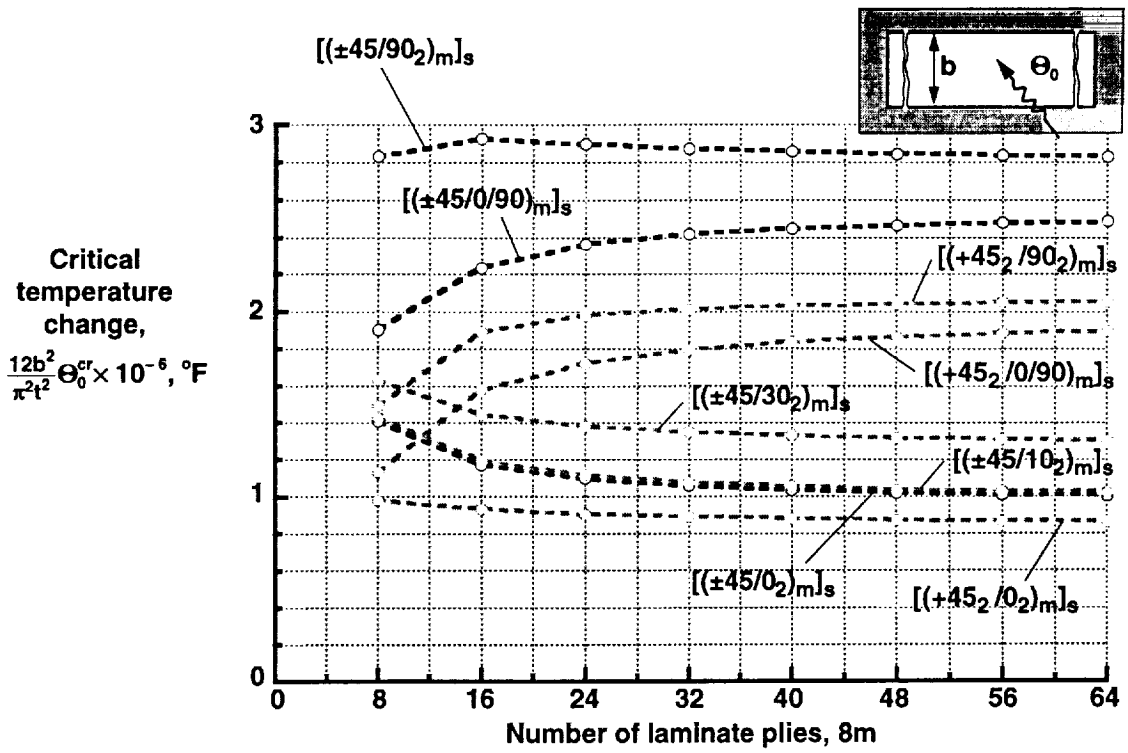

Fig. 10 Critical temperature change for clamped laminates made of IM7/5260 material, fully restrained against thermal expansion or contraction, and subjected to uniform heating.

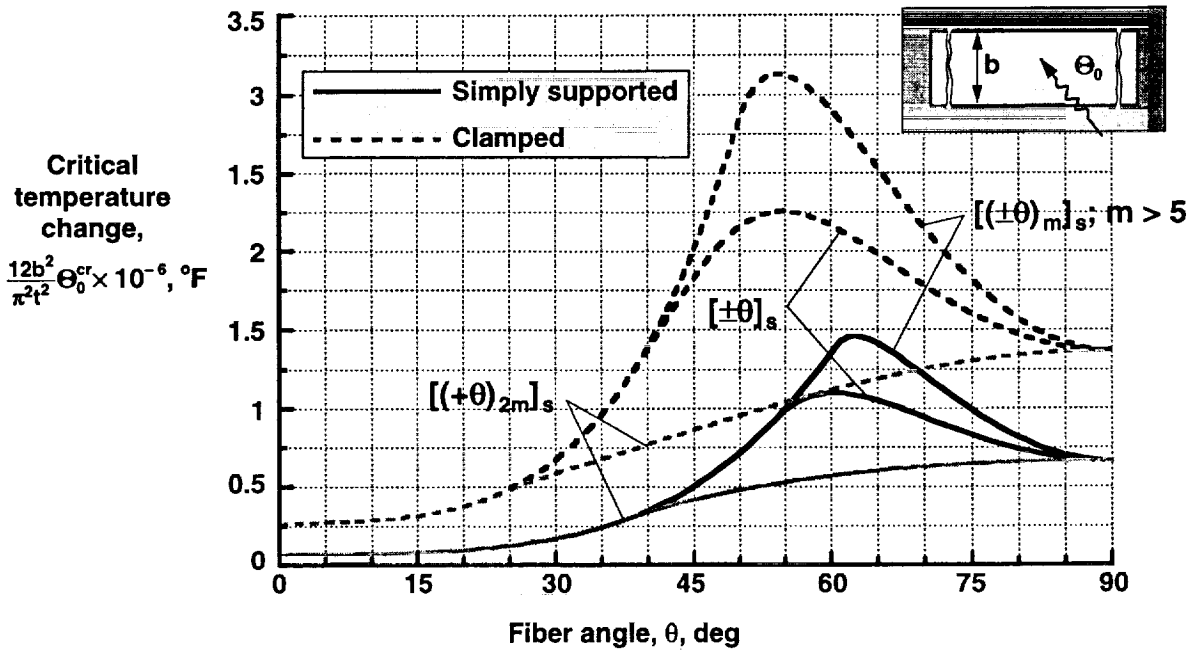

Fig. 11 Critical temperature change for simply supported and clamped angle-ply laminates made of IM7/5260 material (m = 1, 2, ...).

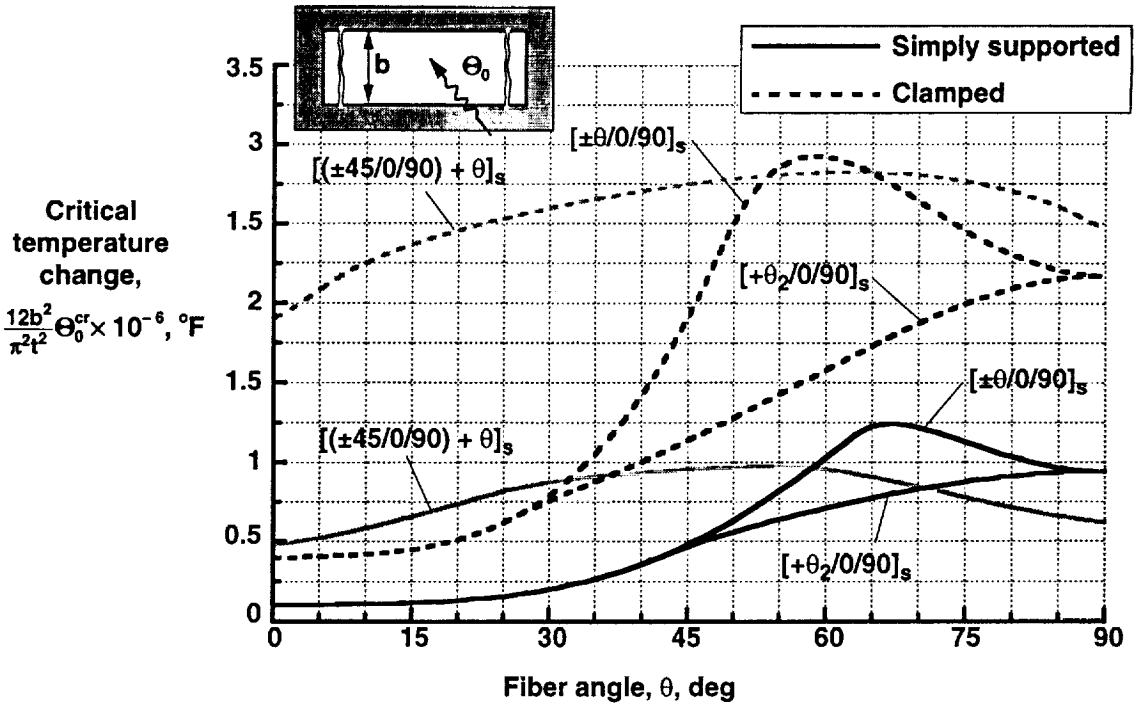

Fig. 12 Critical temperature change for simply supported and clamped laminates with angle-plies made of IM7/5260 material (m = 1, 2, ...).

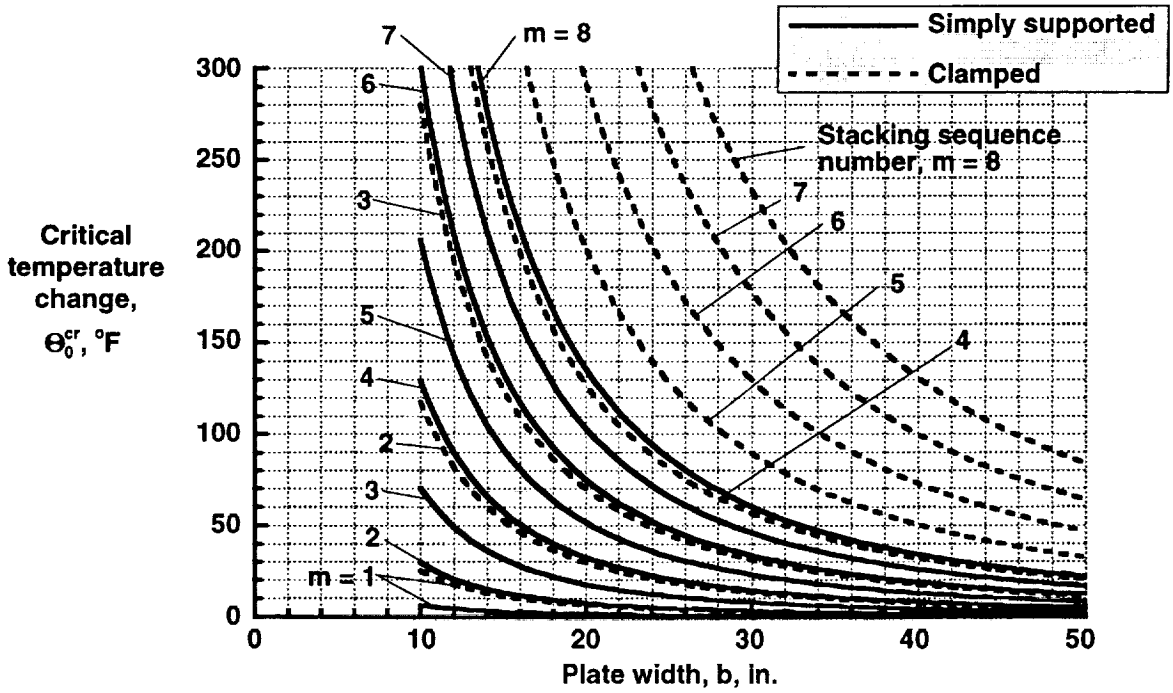

Fig. 13 Critical temperature change versus plate width for simply supported and clamped $[(\pm45/0/90)_m]_s$ laminates made of IM7/5260 material, fully restrained against thermal expansion and contraction, and subjected to uniform heating.

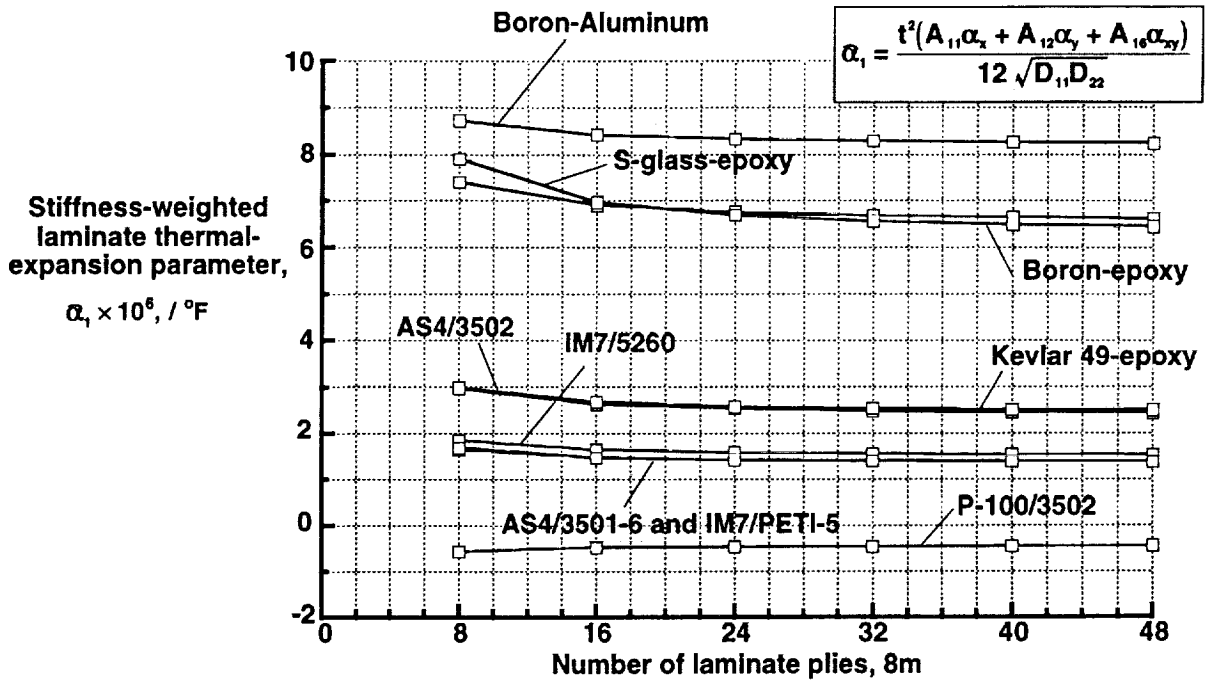

Fig. 14 Effects of lamina material properties on stiffness-weighted laminate thermal-expansion parameter $\bar{\alpha}_1$ for $[(\pm 45/0/90)_m]_s$ laminates.

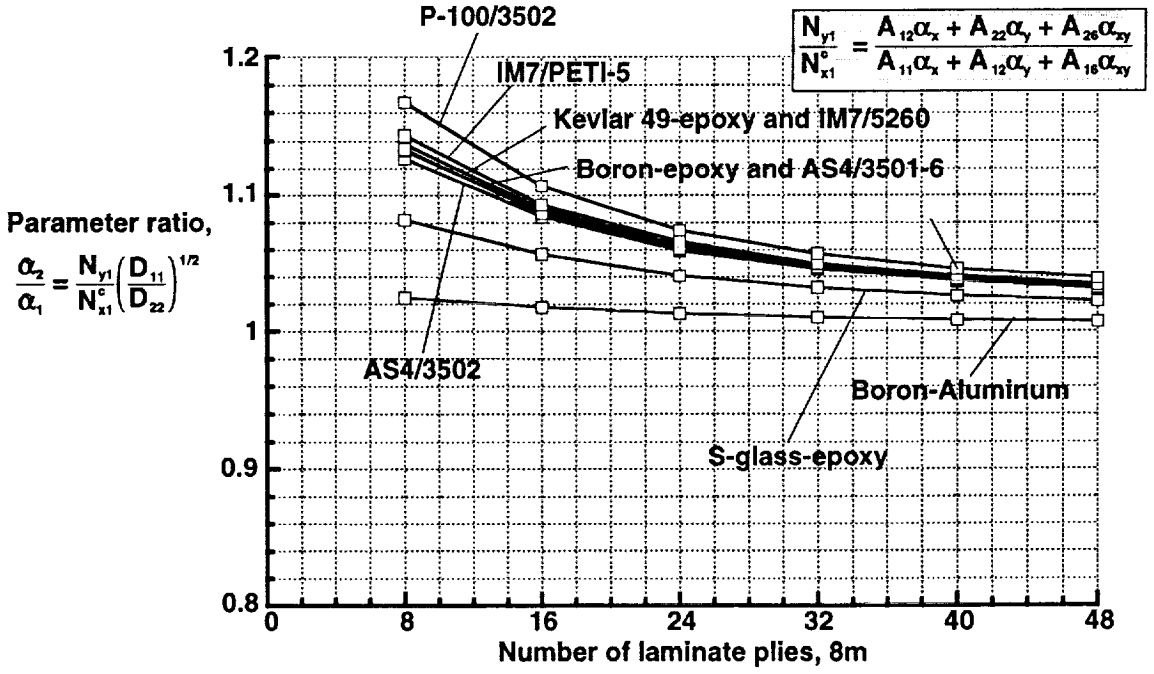

Fig. 15 Effects of lamina material properties on parameter ratio $\bar{\alpha}_2 / \bar{\alpha}_1$ for $[(\pm 45/0/90)_m]_s$ laminates.

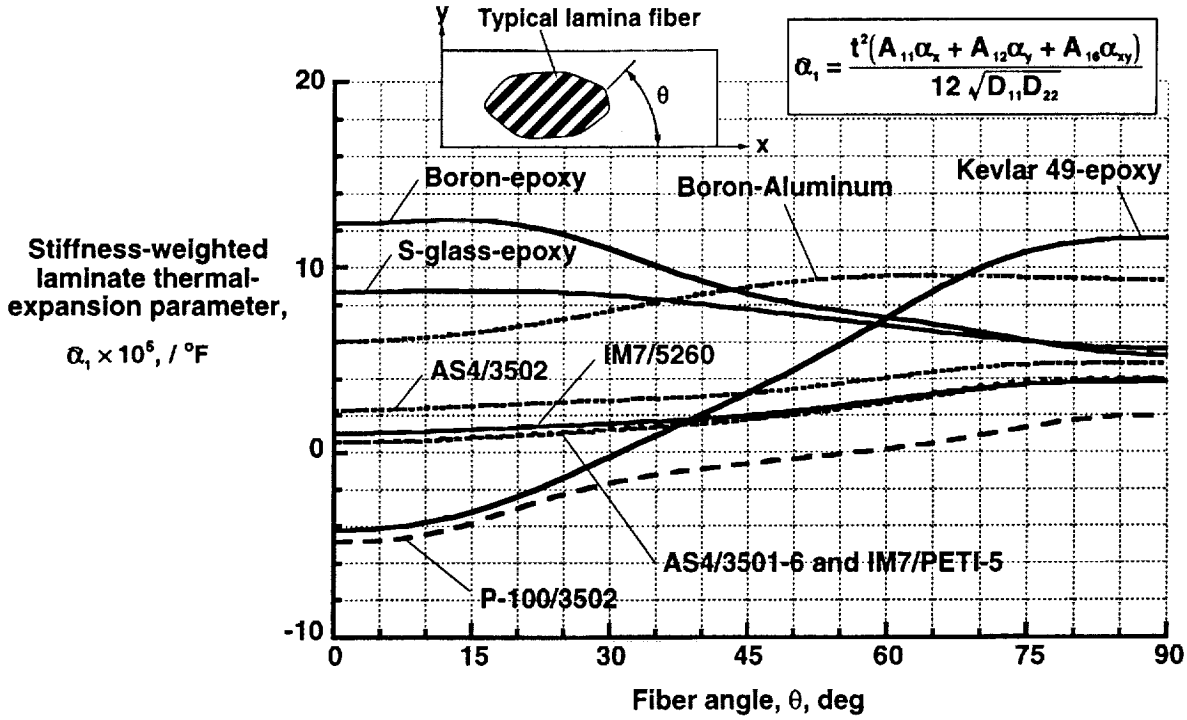

Fig. 16 Effects of lamina material properties on stiffness-weighted laminate thermal-expansion parameter $\bar{\alpha}_1$ for $[(\pm\theta)_m]_s$ balanced, angle-ply laminates and $[(+\theta)_{2m}]_s$ unbalanced, unidirectional off-axis laminates.

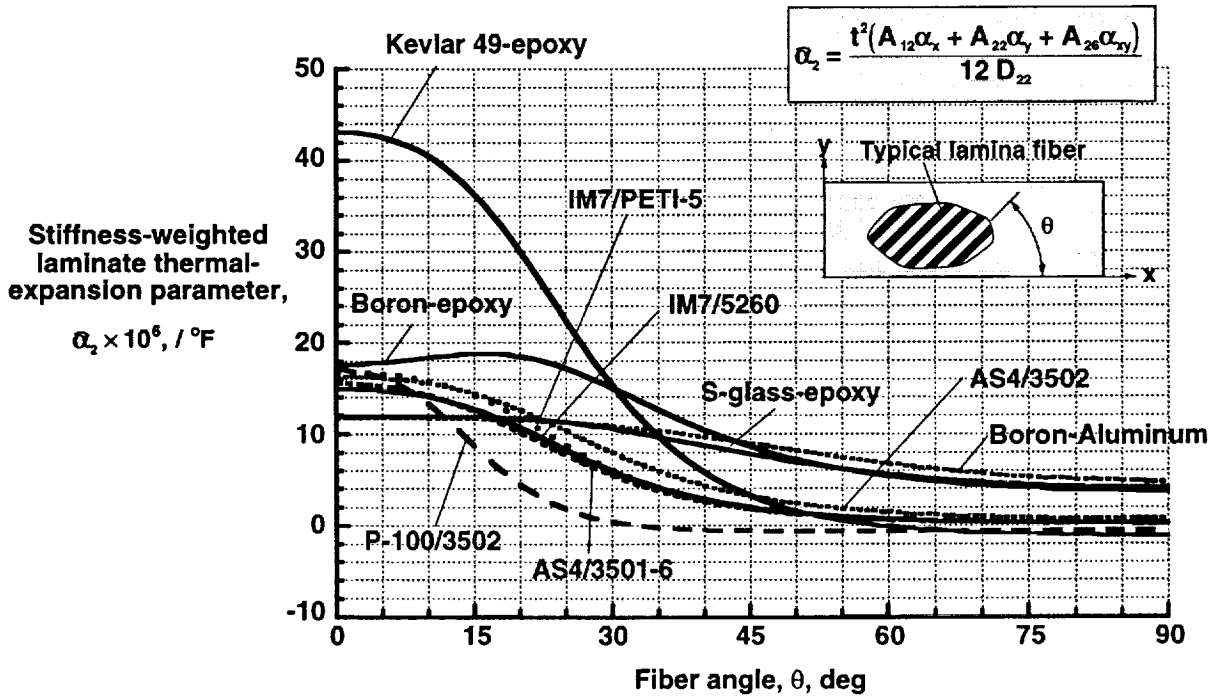

Fig. 17 Effects of lamina material properties on stiffness-weighted laminate thermal-expansion parameter $\bar{\alpha}_2$ for $[(\pm\theta)_m]_s$ balanced, angle-ply laminates and $[(+\theta)_{2m}]_s$ unbalanced, unidirectional off-axis laminates.

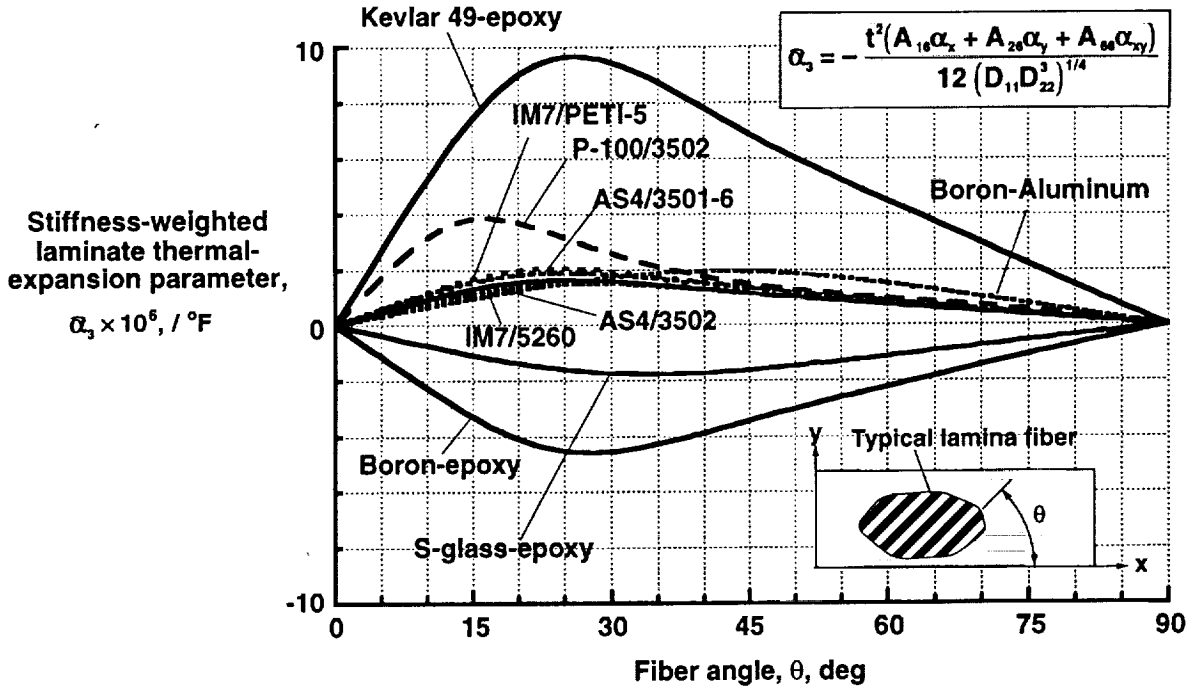

Fig. 18 Effects of lamina material properties on stiffness-weighted laminate thermal-expansion parameter α_s for $[(\pm\theta)_m]_s$ balanced, angle-ply laminates and $[(+\theta)_{2m}]_s$ unbalanced, unidirectional off-axis laminates.

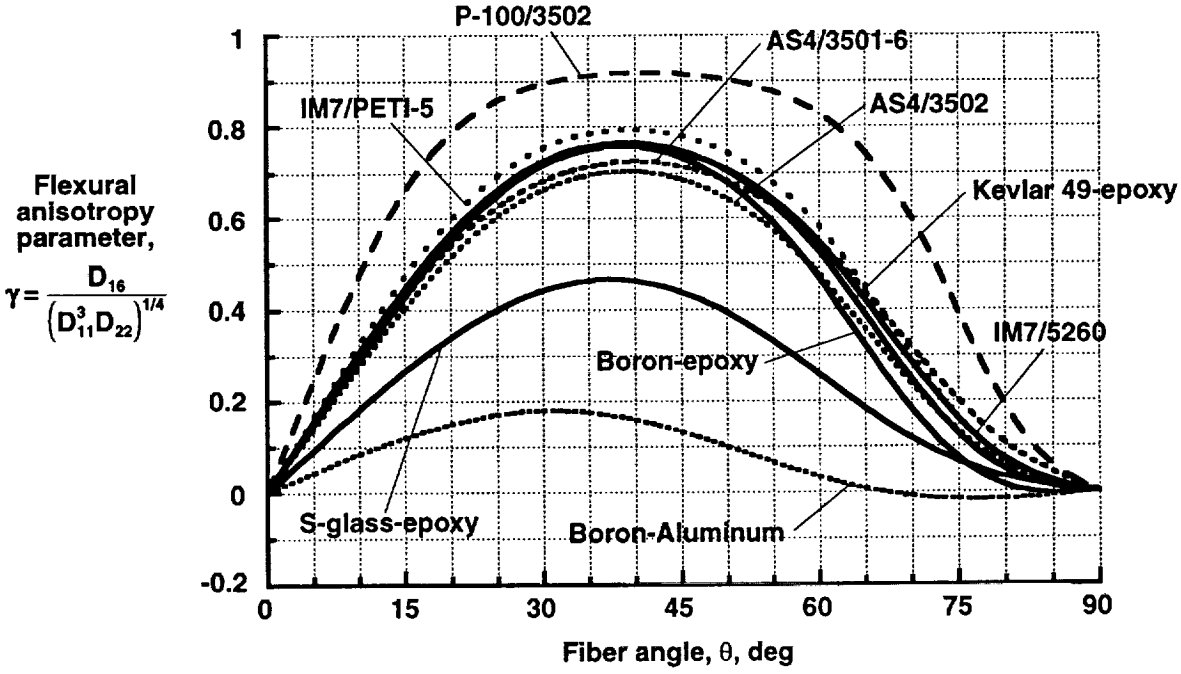

Fig. 19 Effects of lamina material properties on nondimensional flexural anisotropy parameter γ for $[(+\theta)_{2m}]_s$ laminates (m = 1, 2, ...).

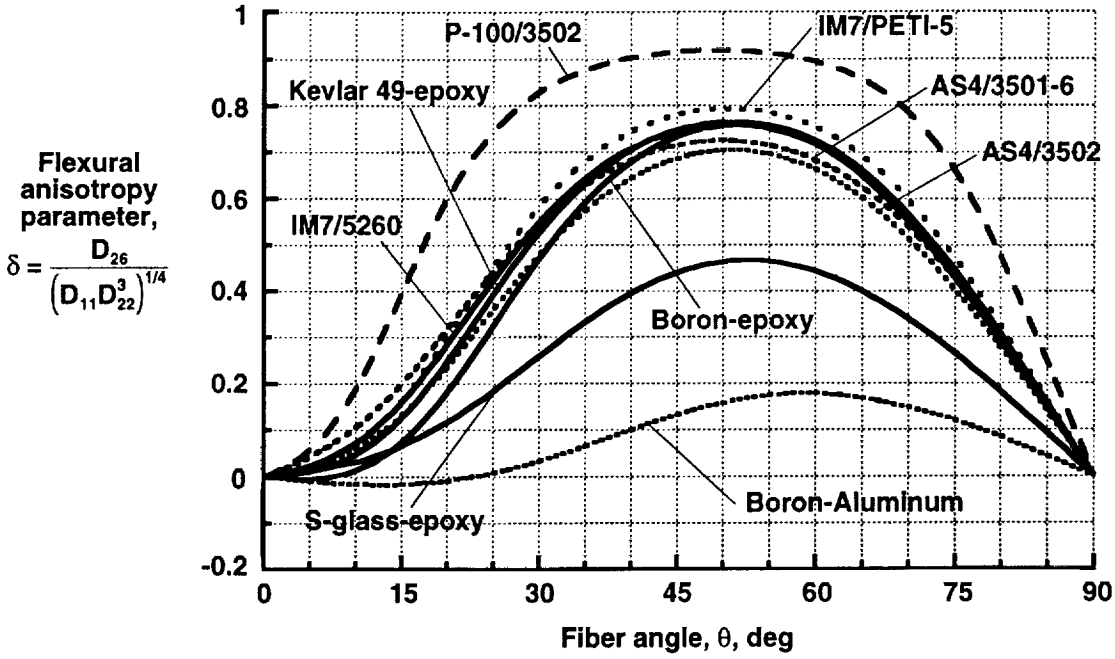

Fig. 20 Effects of lamina material properties on nondimensional flexural anisotropy parameter δ for $[(+\theta)_{2m}]_s$ laminates (m = 1, 2, ...).

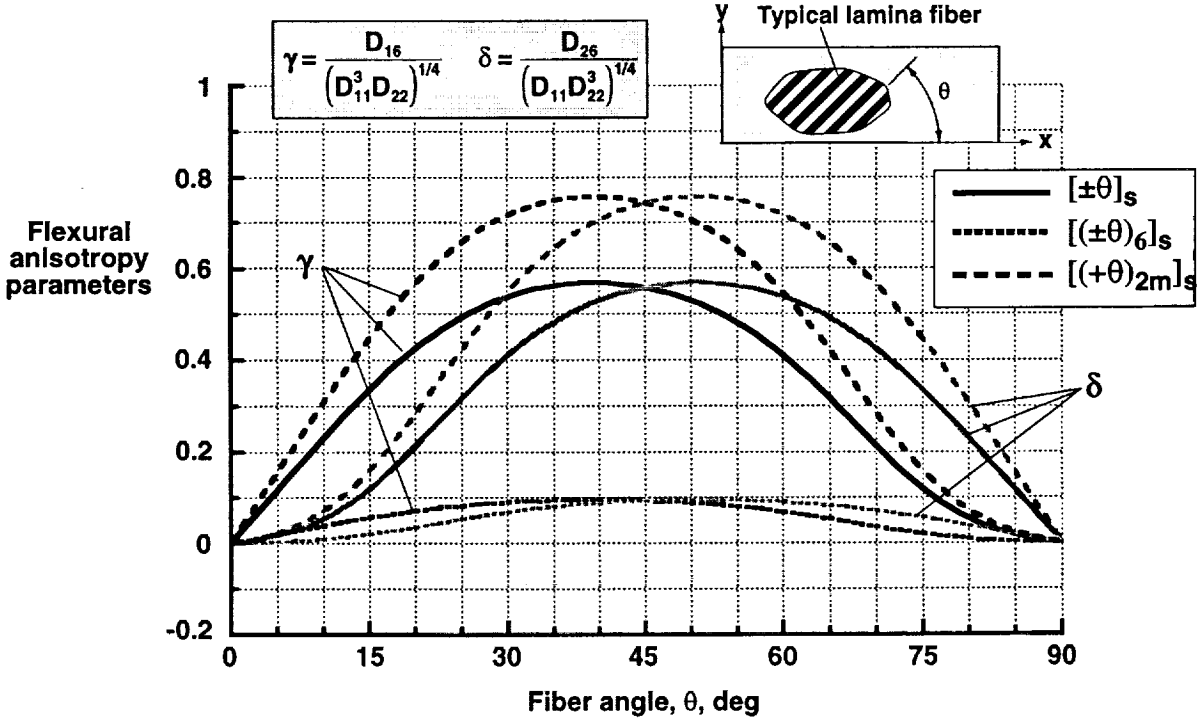

Fig. 21 Flexural anisotropy parameters for angle-ply laminates made of IM7 / 5260 material.

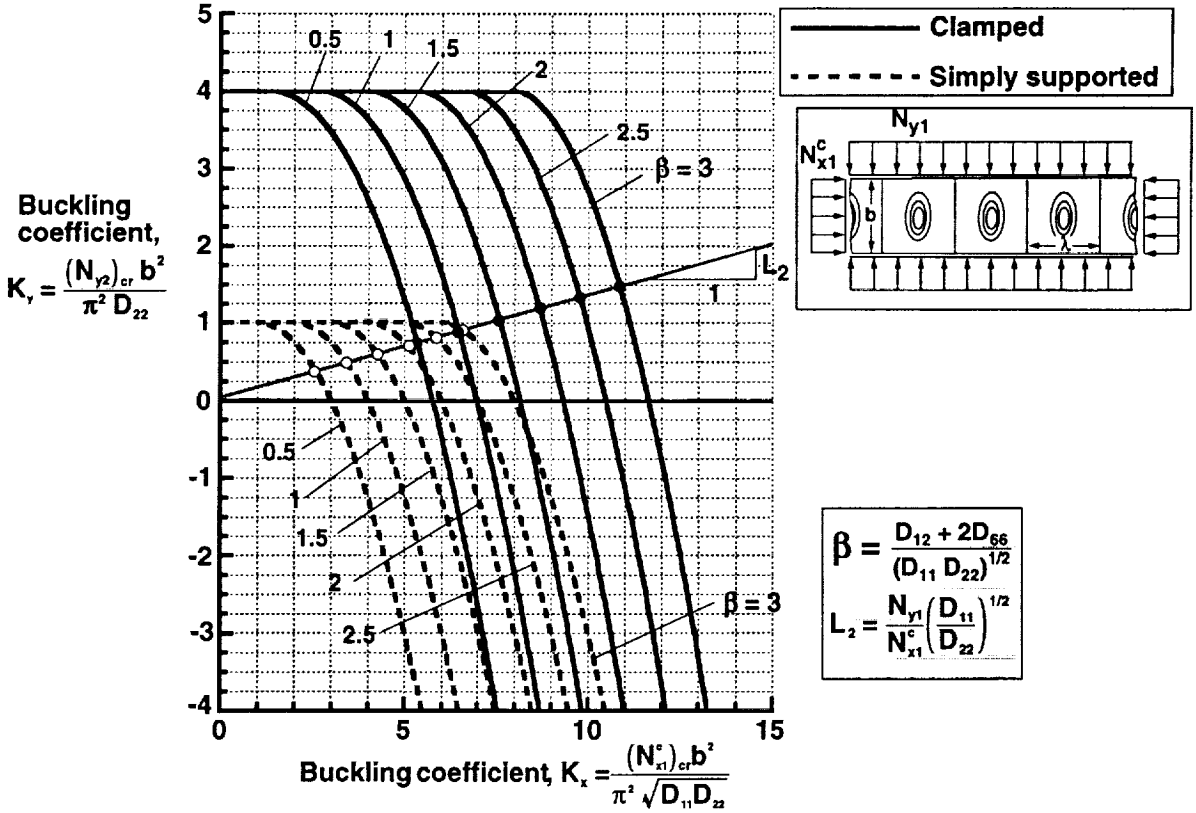

Fig. 22 Effects of orthotropy parameter β on buckling interaction curves for specially orthotropic plates (γ = δ = 0) subjected to axial compression and transverse tension or compression loads.

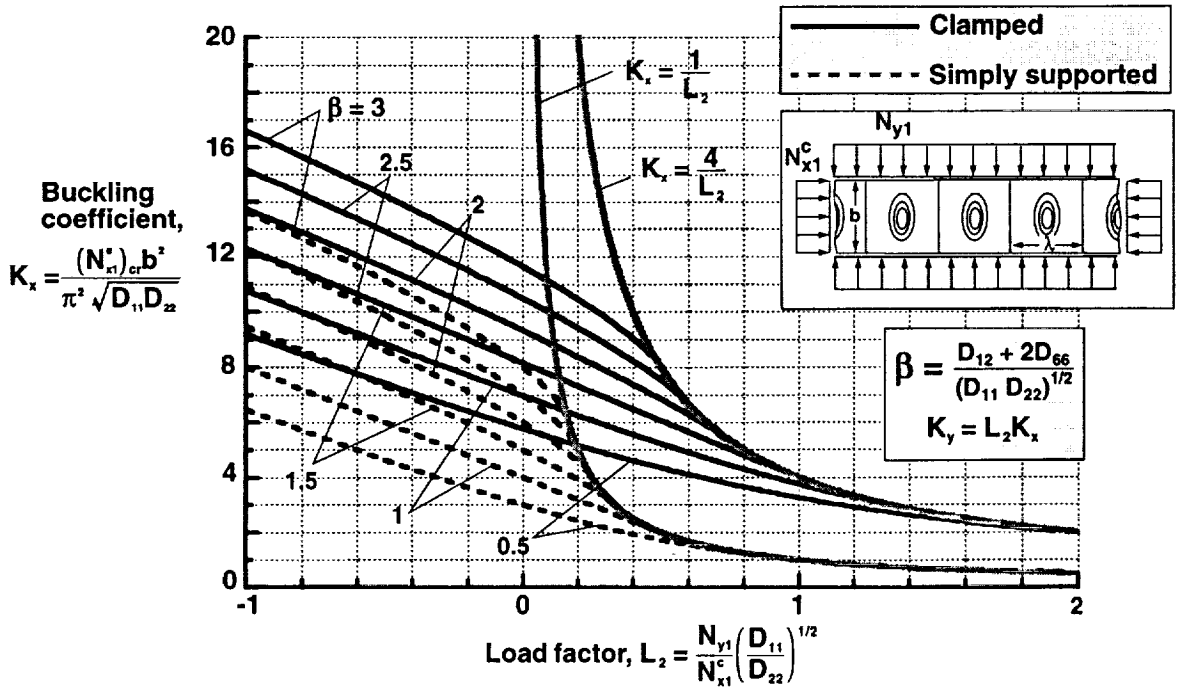

Fig. 23 Effects of orthotropy parameter β and load factor on buckling coefficient for specially orthotropic plates (γ = δ = 0) subjected to axial compression and transverse tension or compression loads.

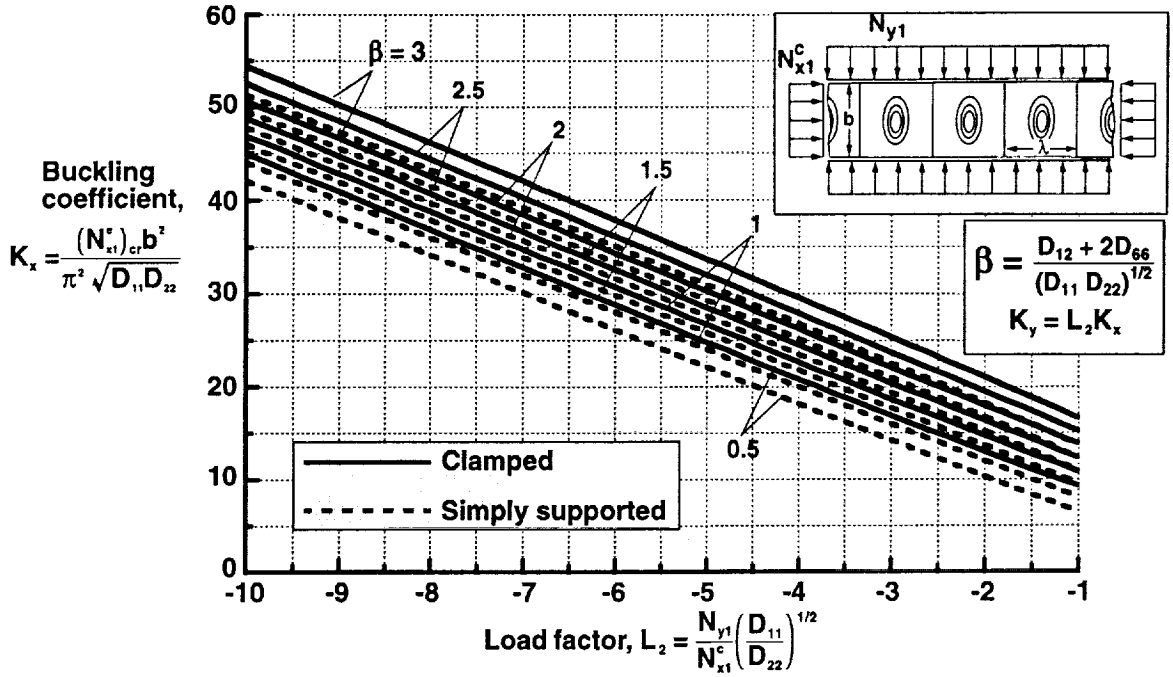

Fig. 24 Effects of orthotropy parameter β and load factor on buckling coefficient for specially orthotropic plates (γ = δ = 0) subjected to axial compression and transverse tension or compression loads.

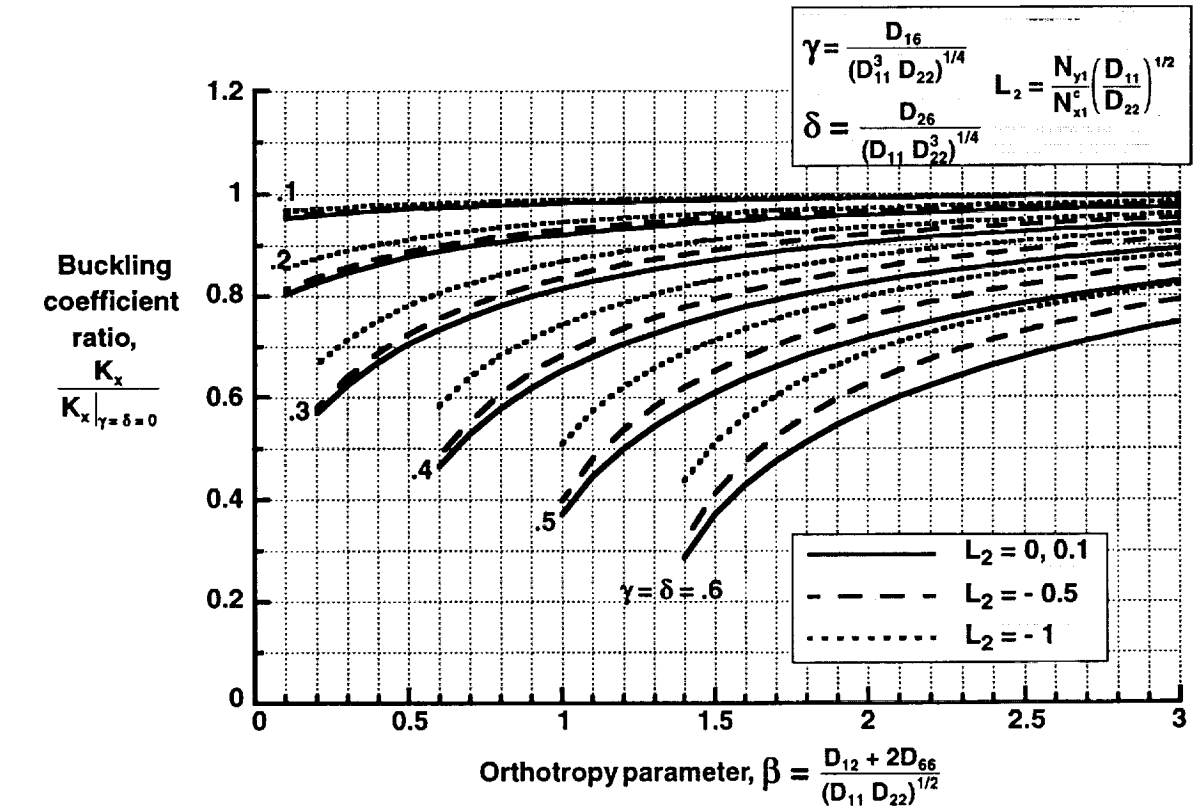

Fig. 25 Effects of flexural orthotropy parameter β and flexural anisotropy parameters γ and δ on buckling coefficients for simply supported plates subjected to axial compression and subcritical transverse tension or compression loads.

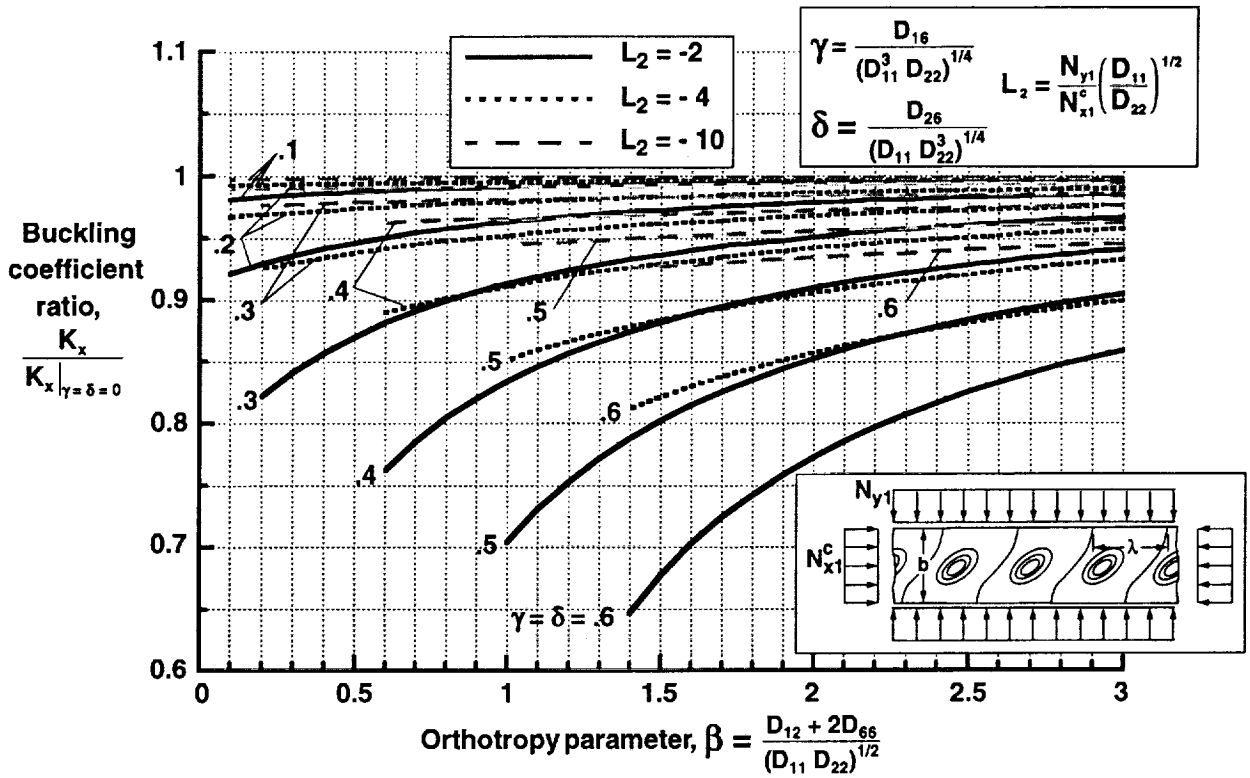

Fig. 26 Effects of flexural orthotropy parameter β and flexural anisotropy parameters γ and δ on buckling coefficients for simply supported plates subjected to axial compression and subcritical transverse tension or compression loads.

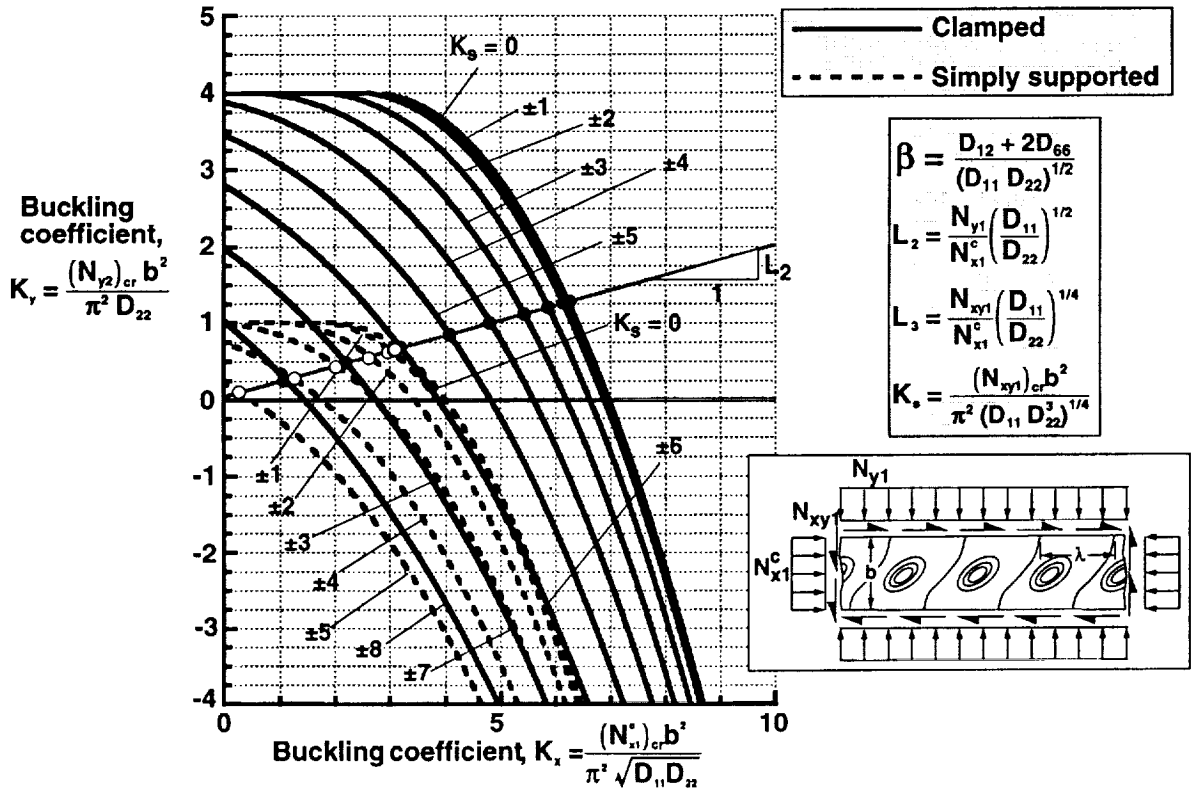

Fig. 27 Buckling interaction curves for specially orthotropic plates ($\gamma = \delta = 0$) with $\beta = 1$ subjected to axial compression, transverse tension or compression, and shear loads.

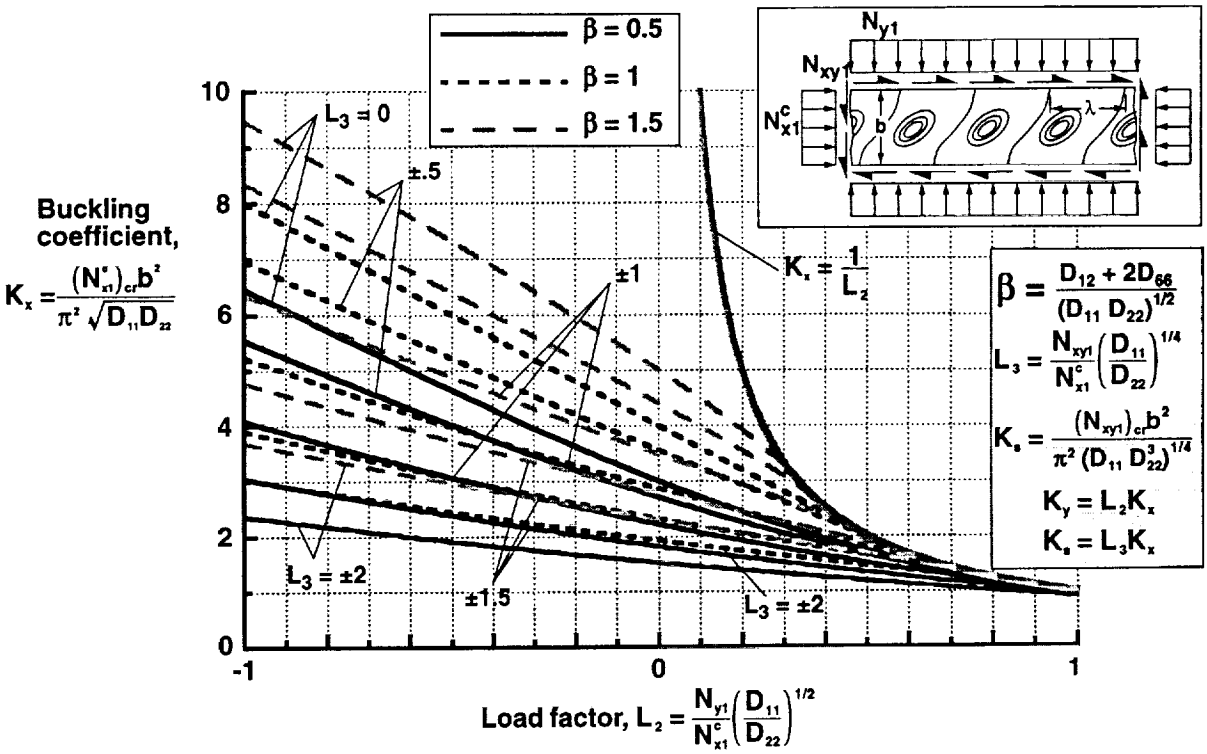

Fig. 28 Effects of orthotropy parameter β and load factors on buckling coefficient for simply supported, specially orthotropic plates ($\gamma = \delta = 0$) subjected to axial compression, transverse tension or compression, and shear loads.

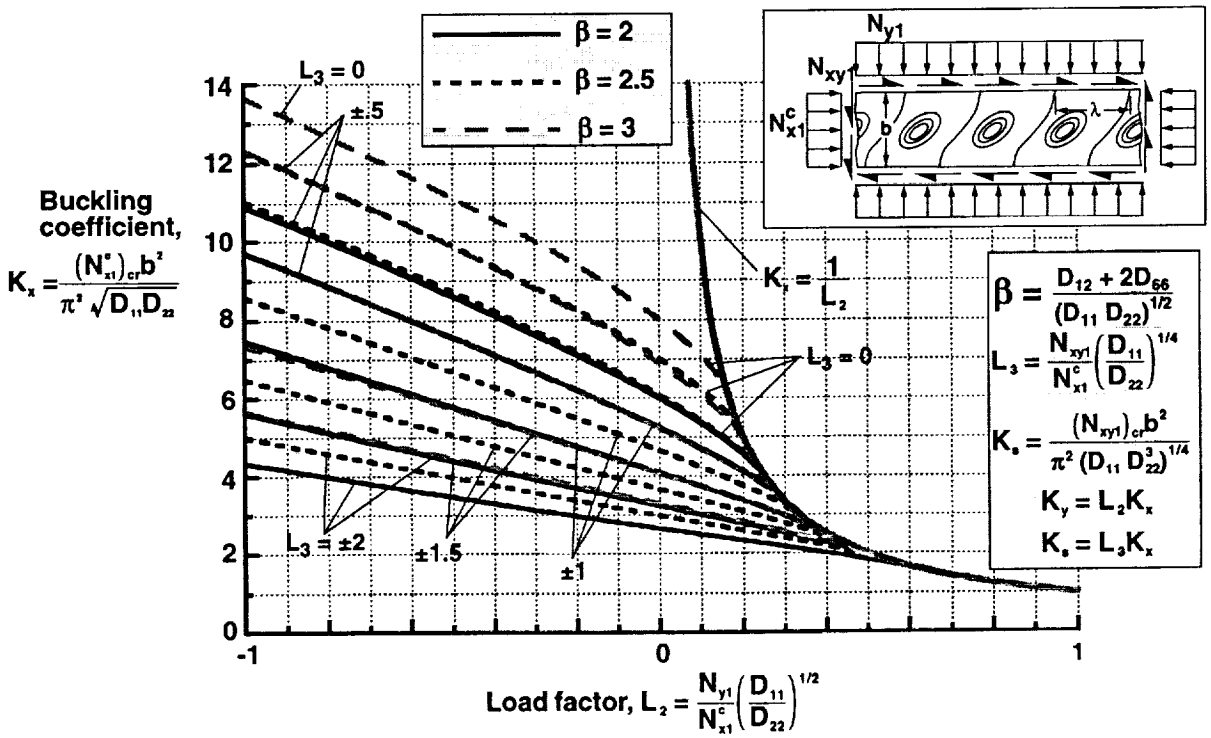

Fig. 29 Effects of orthotropy parameter β and load factors on buckling coefficient for simply supported, specially orthotropic plates ($\gamma = \delta = 0$) subjected to axial compression, transverse tension or compression, and shear loads.

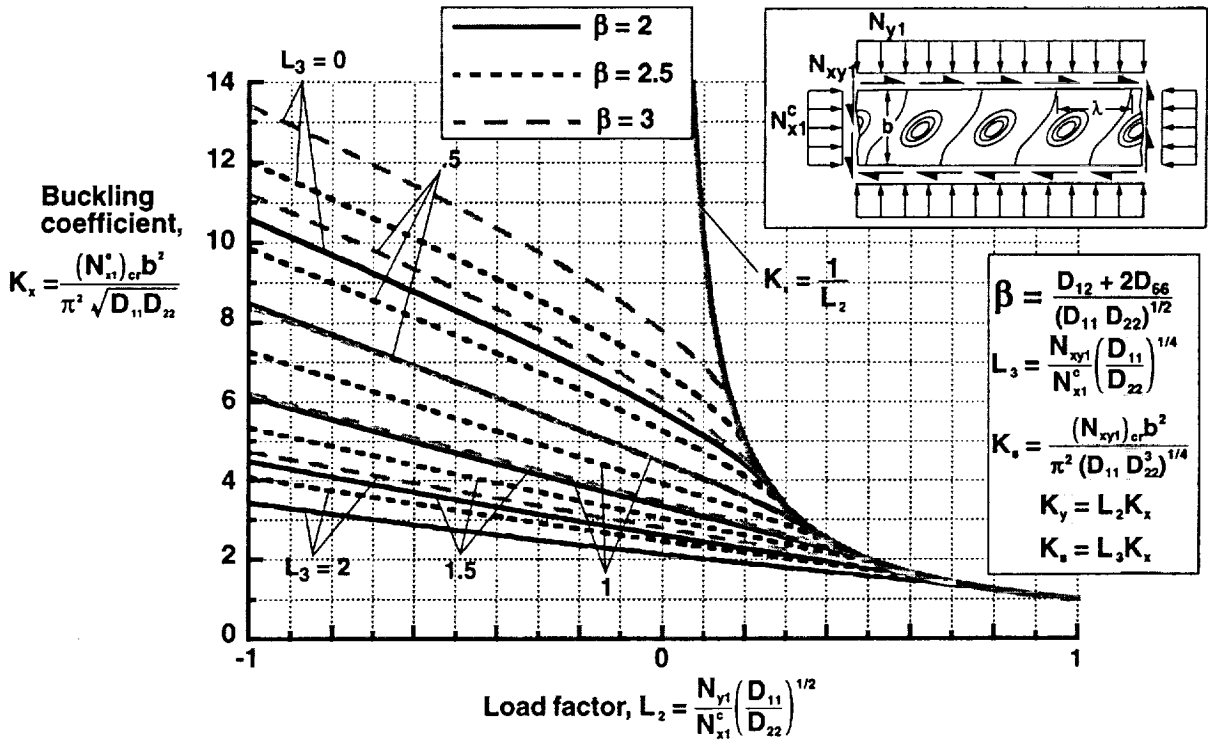

Fig. 30 Effects of orthotropy parameter β and load factors on buckling coefficient for simply supported, specially orthotropic plates (γ = δ = 0.2) subjected to axial compression, transverse tension or compression, and shear loads.

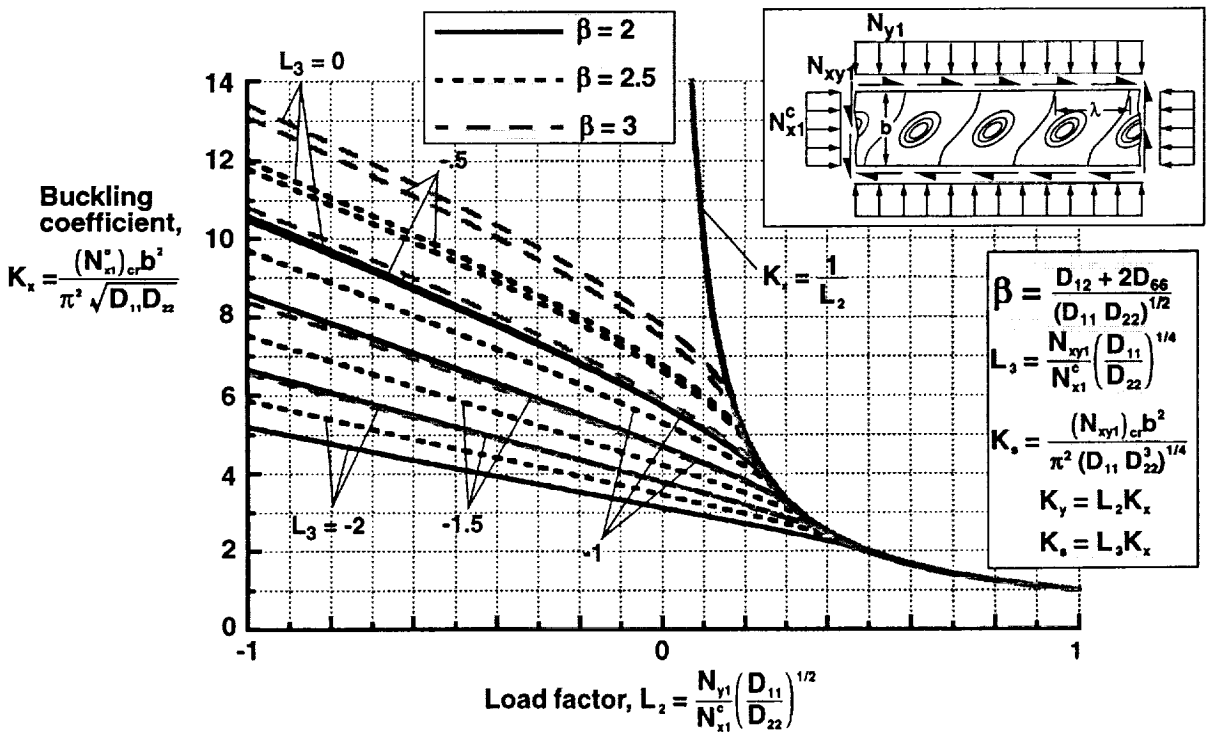

Fig. 31 Effects of orthotropy parameter β and load factors on buckling coefficient for simply supported, specially orthotropic plates (γ = δ = 0.2) subjected to axial compression, transverse tension or compression, and shear loads.

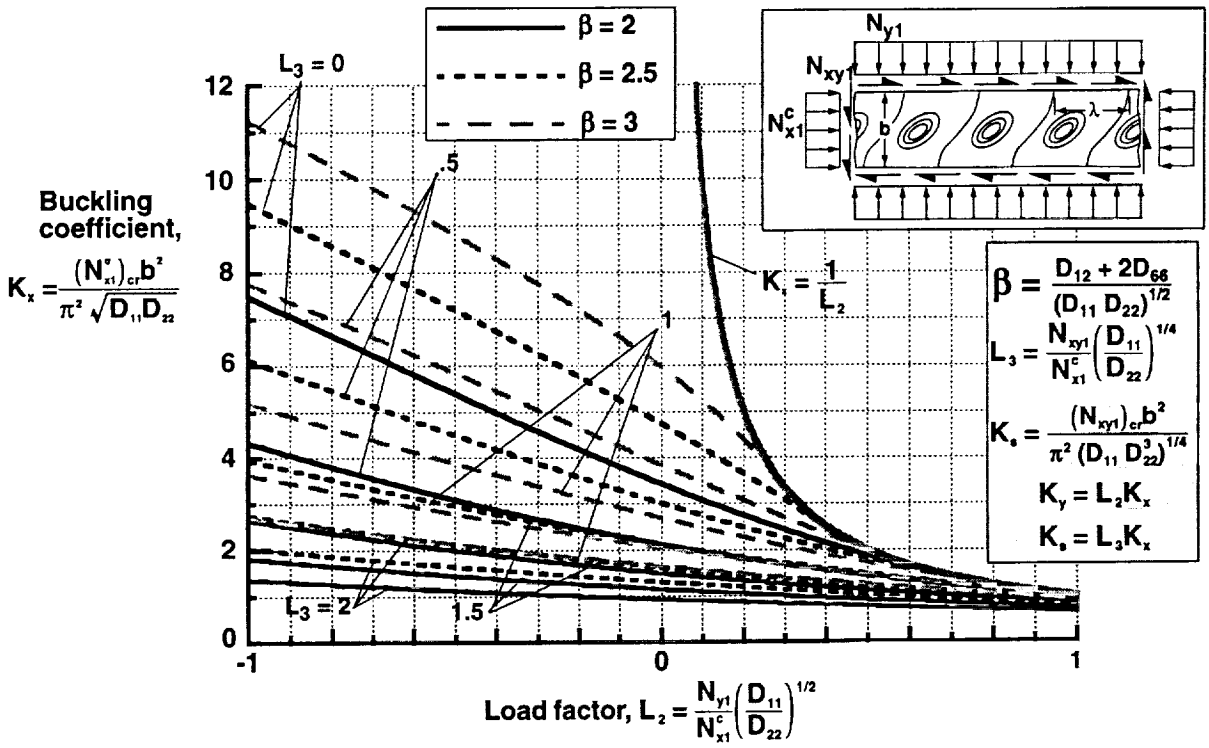

Fig. 32 Effects of orthotropy parameter β and load factors on buckling coefficient for simply supported, specially orthotropic plates (γ = δ = 0.6) subjected to axial compression, transverse tension or compression, and shear loads.

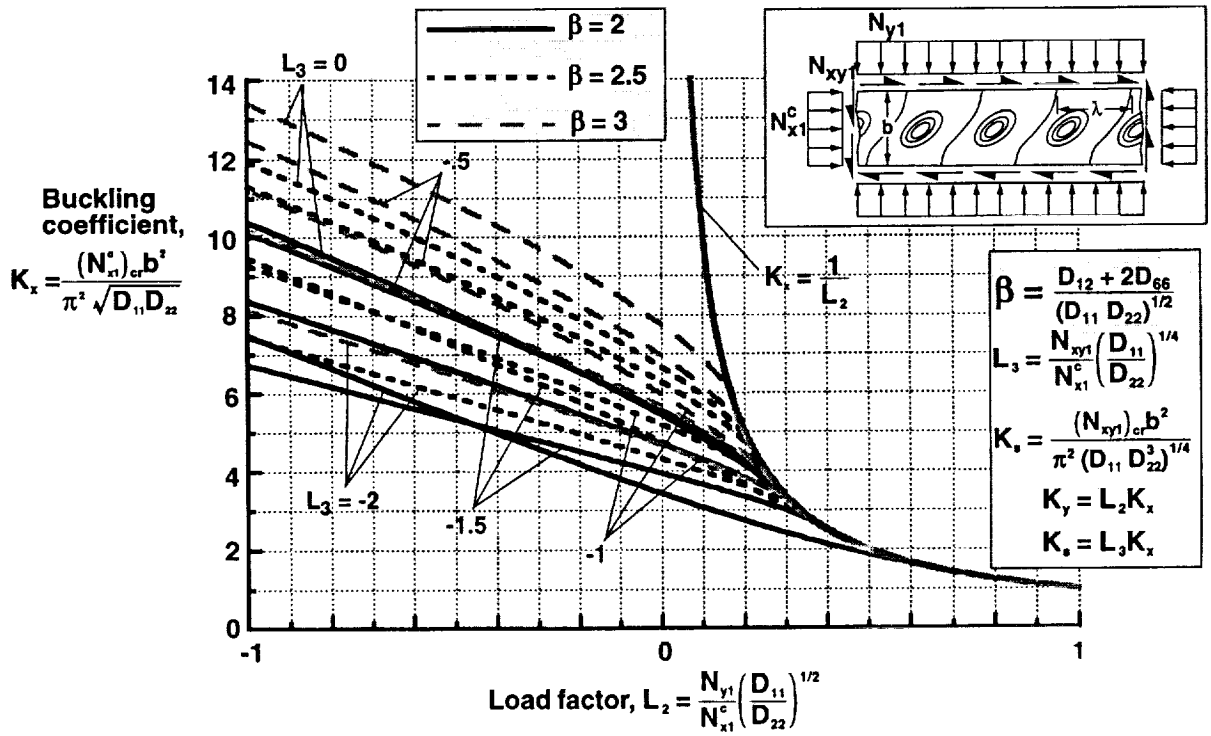

Fig. 33 Effects of orthotropy parameter β and load factors on buckling coefficient for simply supported, specially orthotropic plates (γ = δ = 0.6) subjected to axial compression, transverse tension or compression, and shear loads.